Unsteady State Performance of Porous Gas-Diffusion Electrodes in Alkaline Fuel Cell

by

Abu Ibrahim Inamah

A Thesis Presented to the

FACULTY OF THE COLLEGE OF GRADUATE STUDIES

KING FAHD UNIVERSITY OF PETROLEUM & MINERALS

DHAHRAN, SAUDI ARABIA

In Partial Fulfillment of the
Requirements for the Degree of

MASTER OF SCIENCE

In

CHEMICAL ENGINEERING

December, 1990

INFORMATION TO USERS

This manuscript has been reproduced from the microfilm master. UMI films the text directly from the original or copy submitted. Thus, some thesis and dissertation copies are in typewriter face, while others may be from any type of computer printer.

The quality of this reproduction is dependent upon the quality of the copy submitted. Broken or indistinct print, colored or poor quality illustrations and photographs, print bleedthrough, substandard margins, and improper alignment can adversely affect reproduction.

In the unlikely event that the author did not send UMI a complete manuscript and there are missing pages, these will be noted. Also, if unauthorized copyright material had to be removed, a note will indicate the deletion.

Oversize materials (e.g., maps, drawings, charts) are reproduced by sectioning the original, beginning at the upper left-hand corner and continuing from left to right in equal sections with small overlaps. Each original is also photographed in one exposure and is included in reduced form at the back of the book.

Photographs included in the original manuscript have been reproduced xerographically in this copy. Higher quality 6" x 9" black and white photographic prints are available for any photographs or illustrations appearing in this copy for an additional charge. Contact UMI directly to order.

UMI

A Bell & Howell Information Company
300 North Zeeb Road, Ann Arbor MI 48106-1346 USA
313/761-4700 800/521-0600

NOTE TO USERS

UNSTEADY STATE PERFORMANCE OF POROUS GAS-DIFFUSION ELECTRODES IN ALKALINE FUEL CELL

BY

Abu Ibrahim Inamah

A Thesis Presented to the

FACULTY OF THE COLLEGE OF GRADUATE STUDIES

KING FAHD UNIVERSITY OF PETROLEUM & MINERALS

DHAHRAN, SAUDI ARABIA

In Partial Fulfillment of the
Requirements for the Degree of

MASTER OF SCIENCE

In

CHEMICAL ENGINEERING

December 1990

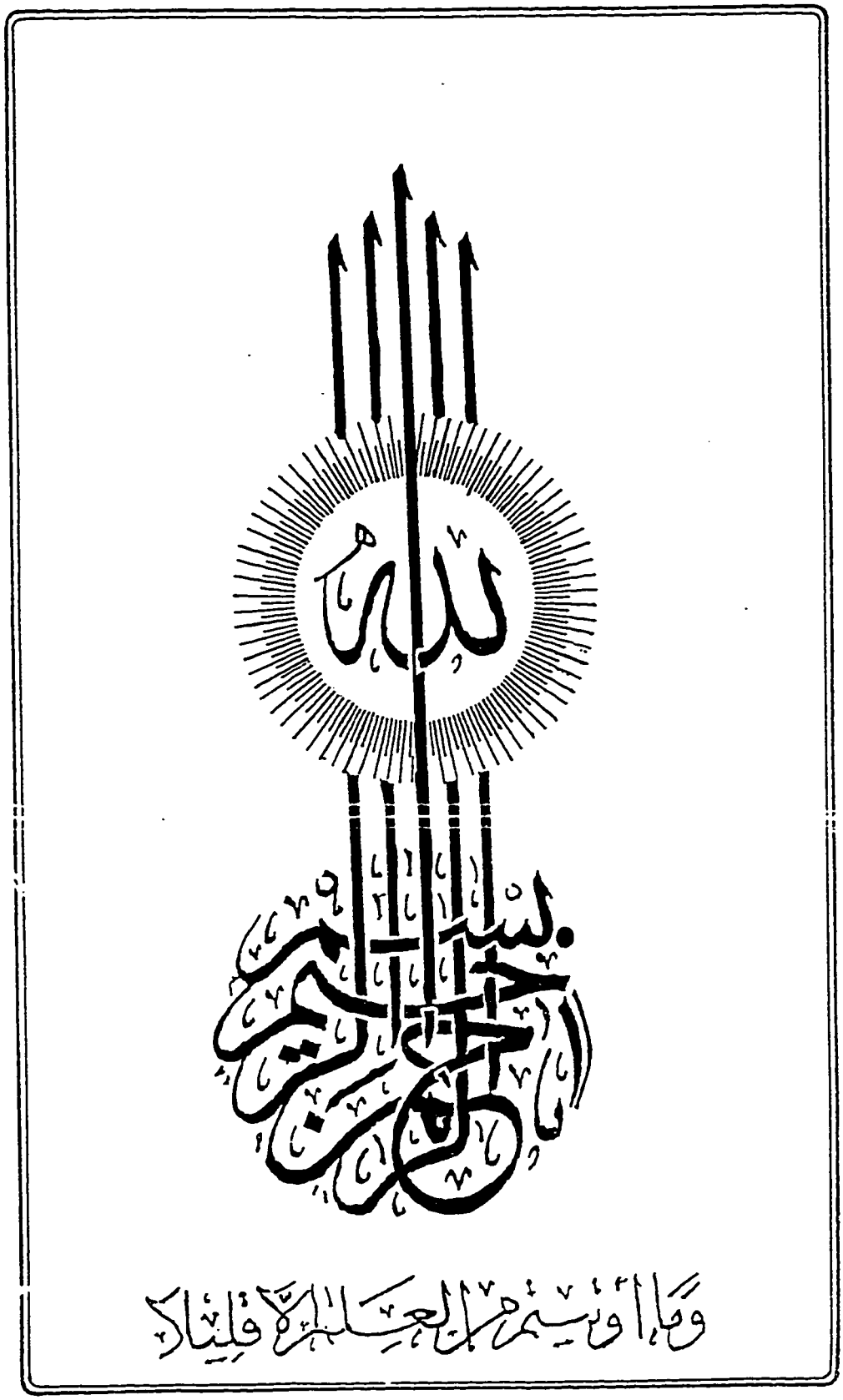
بسم الله الرحمن الرحيم
وما أوتيتم من العلم إلا قليلا

KING FAHD UNIVERSITY OF PETROLEUM AND MINERALS
DHAHRAN, SAUDI ARABIA

COLLEGE OF GRADUATE STUDIES

This thesis, written by Mr. Abu Ibrahim Inamah under the direction of his Thesis Advisor and approved by his Thesis Committee, has been presented to and accepted by the Dean of the College of Graduate Studies, in partial fulfillment of the requirements for the degree of MASTER OF SCIENCE in Chemical Engineering.

Thesis Committee:

Dr. Selahattin Gultekin
Thesis Advisor

Dr. Mohammad A. Al-Saleh
Member

Dr. Abdullah S. Al-Zakri
Member

Dr. M.A. Shalabi
Department Chairman

Dr. Ala H. Al-Rabeh
Dean, College of Graduate Studies

Date: March 2, 1991

Dedicated to :

My Parents, Wife and all Peace-loving people

ACKNOWLEDGEMENTS

First of all, I would like to thank the Almighty Allah for giving me the strength and power throughout my stay in this university.

I am also highly indebted to the University of Petroleum & Minerals, which gave me the opportunity and support in my Graduate Studies.

I would like to deeply thank my thesis advisor, Dr. Selahattin Gultekin for his excellent guidance and admirable inspiration. Thanks are also due to the other committee members, Dr. Muhammed A. Al-Saleh and Dr. Abdullah S. Al- Zakri for their marvelious assistance and generousity. I appreciate that highly.

I acknowledge the timely assistance of the technicians at the Chemical Engineering Department especially Mr. Jim Butcher, Mr. Ibrahim and Mr. Maher. I would also like to extend my appreciation to all those people who have in one way or another contributed towards the positive realisation of this thesis work.

TABLE OF CONTENTS

CHAPTER 3: LITERATURE REVIEW

CHAPTER 4: EXPERIMENTAL SECTION

CHAPTER 5: RESULTS AND DISCUSSION

CHAPTER 6: CONCLUSIONS AND RECOMMENDATIONS

LIST OF TABLES

LIST OF FIGURES

Figure *Page*

ABSTRACT

FULL NAME OF STUDENT: ABU IBRAHIM INAMAH

TITLE OF STUDY:UNSTEADY STATE PERFORMANCE OF POROUS GAS-DIFFUSION ELECTRODES IN ALKALINE FUEL CELL

MAJOR FIELD : CHEMICAL ENGINEERING

DATE OF DEGREE : DECEMBER 1990

The unsteady state method of employing exponential decay current was used to determine the performance of the hydrogen electrode of the alkaline fuel cell. A triangular wave technique was also carried out in a separate investigation in order to compare the results with that of the exponential decay current. The study was undertaken in a half-cell. The fuel was pure hydrogen and the electrolyte was a 25% solution KOH. The electrode used was a Raney-Nickel supplied by DLR of Germany. The experiments were carried out for the temperature range of 30°C – 65°C. In the exponential current technique, the input currents were generated from the discharge of capacitors of different sizes. The responses of the fuel cell to the input currents were then analysed to determine the intrinsic parameters such as the exchange current densities i_o, and the double layer capacitances C_T. The activation energy and the surface roughness factors were also determined. The ranges of values obtained for the exchange current densities and the double layer capacitance were $(1.05-11.9)\times10^{-6}$A/cm^2 and $(91\text{-}104)\times10^{-3}$F respectively for the temperature range of the investigation. The activation energy was found to be 4.15 kcal/gmol and the surface roughness factor at 65°C was 34×10^{-4}cm^2/cm^2. It was realised that both the exchange current density and the surface roughness factor were high while the activation energy was low compared to that reported earlier in the literature. These results showed that the electrodes have better performance due to the improved preparation techniques. An increase in temperature also promoted more electrochemical reactions to take place resulting in the increase of the performance of the fuel cell.

MASTER OF SCIENCE DEGREE

KING FAHD UNIVERSITY OF PETROLEUM AND MINERALS

Dhahran, Saudi Arabia

Date : December 1990

خلاصـــــــــة

اسم الطالب كامـــلا : ابو ابراهيم اناماه

عنوان الدارســـــة : الاداء الغير مستثمر للاقطاب مسامية انتشار الغاز في خلية الوقود القلوية

التخصـــــــــص : هندسة كيميائيـــــــــة

تاريخ الشهـــــادة : ديسمبـــــر ١٩٩٠م

لقد استعملت طريقة تلاشي التيـــار الاس في تقييم اداء قطب الهيدروجين خلية الوقود القلـــوية ٠

ولقد استعملت ايضا طريقة الموجـــة المثلثـة في بحث مستقل لمقارنه النتائج مع تلك الناتجـــة عن طريقة تلاشـي التيـــار الاســـي ٠ وتمـت الدراســة في نصف الخلية ٠

ولقد استخدم الهيدروجين فقط كوقود والالكتروليت كان عبارة عن ٢٥ ٪ من محلول البوتاسـيوم هيدروكسيد والقطب المستخدم كان (Raney - Nickel) زود بواسطة DLR الالمانية ٠

ولقد تمت التجارب عند درجة حرارة مابيـن ٣٠ الي ٦٥°م ٠ بالنسـبة لعمليـة التيار الاســي، فقد تم توليد التبارات الداخلة من تفريغ مكثفات ذات احجام مختلفة ٠ ثم تم تحليل اســتجابات خليه الوقـود للتبارات الداخلة وثم ايجـاد مقادير مثل كثافـة التيار (i_o) والمواسعات ثنائية الطبقات (C_T) تم ايضا تحـديد قيمـة الطاقـة المحفزة و معامل خشونه السـطح ٠

ولقد وجد أن قيمة كثافة التيار والمواسعات ثنائية الطبقة عند درجـات الحرارة المستخدمة (٠٥ر١-٩ر١١)× ١٠ $\frac{mA}{cm^2}$ و (٩١ ـ ١٠٤) × ١٠$^{-٣}$ F علي التوالي ٠

وجـد ان مقدار الطاقـة المحفزة كان ٤ر١٥ $\frac{Kcal}{gmol}$ ومعامل خشـونه السـطح عند درجة حرارة ٦٥°مئوية كان يساوى ٤٣× ١٠$^{-٤}$ سم ٢ ٠ ولقد وجـد ان كلا من كثافة التيـــارو معامل خشونه السطح كانـا عاليـا بينمـا الطـاقة المحفزة كانت منخفضـــة بالنسـبة الي القيـم المنشوره ســابقا ٠

أثبتت هـذه النتائج بأن الاقطـاب تتمتع باداء افضـل نتيجـة لطرق اعدادهـا المحسنة ٠

ولقد عززت الزيـــادة في درجـة الحـرارة حدوث تفاعلات كهروكيميائية وينتج عنها زيادة في فاعليـة خليـة الوقود ٠

درجة الماجستير في العلوم

جامعة الملك فهد للبترول والمعادن

الظهران ، المملكة العربية السعوديـــــــة

التاريخ : ديسمبر ١٩٩٠م

LIST OF SYMBOLS

A : cross-sectional area

$A_1 = \frac{n^2\pi^2 + \alpha}{\beta}$

$B = \frac{\alpha}{\beta}$

C:Differential Capacity per cm^2

C_i^v: Equilibrium concentration.

C_{ideal} : Double layer capacitance for ideal nickel surface.

Co : Initial reactant concentration

C_p : Initial concentration of products.

C_T : S c L (total Differential Capacity)

D_R: Diffusion coefficient of reactants.

D_P : Diffusion coefficient of Products.

Ea : Energy of activation

Ee : Equilibrium potential

I : i S L (totalcurrent)

i : microkinetic current density ($\frac{i_o n F \eta}{RT}$)

i_o : Exchange Current Density

i(t) : Current density after time t

K : Equlibrium Constant

k_f : Forward Rate Constant

k_b: Backeard Rate Constant

L : pore-length

MW : Power (Mega Watts)

P : Period of Triangular wave

RF : Surface roughness factor

$R_o = \frac{l}{\sigma A}$

S : Surface area of porous electrode per unit length

T : Absolute temperature

t : Temperature deg. C

v : Potential Sweep rate

W : Weight percent concentration of KOH

Greek Letters

$\mu(\frac{amp}{s})$: is the constant rate of change of applied current.

σ : Conductance of KOH solution ($\Omega^{-1} cm^{-1}$)

$\alpha = R_o S L n F \frac{i_o}{RT}$

$\beta = R_o C_T$

$\zeta = \frac{x}{l}$ (Dimensionless length)

$\lambda = \frac{R T K}{nFv}$

ΔG : Change in free energy of the system

CHAPTER 1

1. INTRODUCTION

1.1 Definition of Fuel Cell

A fuel cell is an electrochemical device that directly converts the chemical energy associated with a fuel such as hydrogen or hydrogen-rich gas into direct current electricity. The oxidant gas is usually air but pure oxygen can be used for some applications. Figure 1.1 illustrates the fuel cell process. An electrode is usually required to effect the conversion. The reactants are continuously supplied to the electrodes where electrochemical reactions take place. Simultaneously, fuel is supplied to the fuel compartment(anode) and oxidant supplied to the oxidant compartment (cathode). In order to obtain useful work from the reaction, the electrode processes are physically seperated. The seperation prevents shortcircuiting that could arise if the fuel and oxidant reacted directly. Shortcircuiting does not produce useful electrical energy. Oxidation takes place at the fuel electrode and reduction at the oxidant electrode. A potential difference is created when these electrochemical reactions occur. Consequently, electron flow is promoted that can be taken by an external load to provide useful work. Under the operating conditions of the fuel cell the electrodes should be stable and should not be affected by both the reaction and the electrolyte. The reaction product must be removed to keep the electrolyte invariant.

Theoretically, many chemical reactions are suitable for the the fuel cell operations. However, attention has been given to combustion reactions. The reasons are probably due to the unlimited supply of oxygen and the variety of

options available for the fuel cell compartment.

Under ideal conditions, a fuel cell using conventional fuel and oxygen is capable of giving only one volt. In practice, the desired voltage is achieved by using a fuel cell stack consisting of an assemble of several fuel cell units in series. In the fuel cell system, there is an additional stack and a power conditioning unit for regulating the voltage and converting the direct current into alternating current.

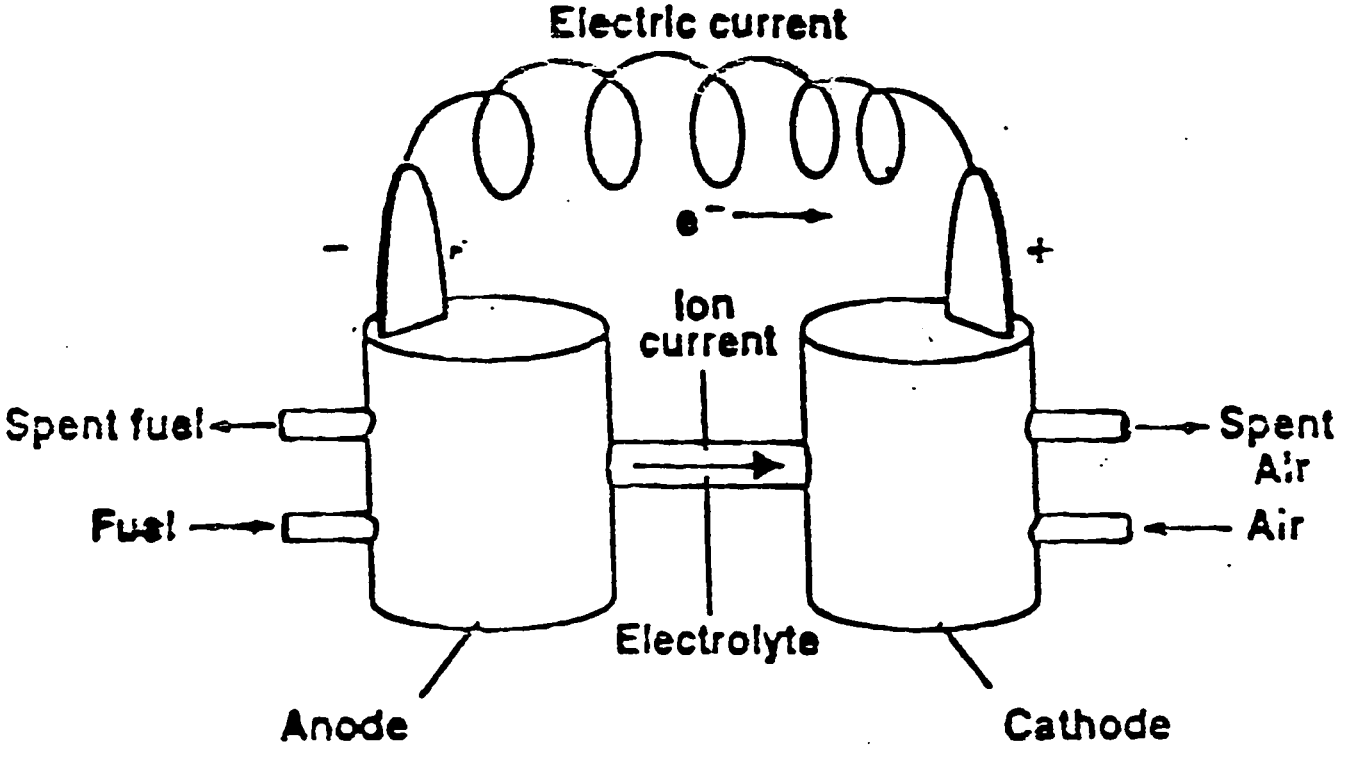

Figure 1.1: Schematic Representation of the Fuel Cell.

1.2 Advantages of Fuel Cells

The major importance of the fuel cell is that it has the potential for supplying clean energy with a unique freedom from the heat engine and its associated limitations of the Carnot's cycle. As a result, the demonstrated effeciencies of fuel cells are considerably higher than other conventional energy conversion devices.

Intrinsic

A number of intrinsic advantages of fuel cells have been given by Young[1]. These advantages include a high efficiency, a minimal number of moving parts and consequently low noise, high reliability, low operating costs and low pollution levels. Other advantages are easy adaptability to operate at any desired temperature range, multifuel capability and fast start up times for the case of low temperature alkaline fuel cells.

Environmental

The essential emissions for fuel cell devices for modern power plants were discussed at a symposium on energy production processes[2] and presented as shown in table 1.1. It can be observed that except for the carbon monoxide where the emissions are equivalent, the others show higher emission rates coming from diesel and gas engines as compared to fuel cells.

Table 1.1: Power Generator Emissions.[17]

Emissions	Diesel	Gas Engine	Gas Turbine	FC
NO_2	30.2	23.0	35.8	0.7
SO_2	4.4	3.5	5.1	0.05
HC	0.9	0.8	1.1	0.20
CO	0.5	0.4	0.7	0.46
particles	2.3	2.1	2.9	0.2

All quantities are measured in Kg/MW-Day

FC : Fuel Cell

Modularity

Fuel cells are suited for mass production since they are intrinsically modular devices consisting of an assembly of a battery of many identical cells. This alleviates costs as compared to long term planning and financing of conventional power plants.

Efficiency

The main advantage of the fuel cell is its high efficiency as compared to conventional combustion driven energy sources. The maximum theoretical efficiency obtainable from heat engines is 40-50%. However for fuel cells, the maximum theoretical efficiency ranges from 70-90%. Benjamin et al [3] combined fuel cells and waste heat for cogeneration and state that the efficiency of the fuel cell was significantly enhanced. Table 1.2 shows the demonstrated efficiencies of direct energy conversion devices.

Disadvantages of the Fuel Cell

The disadvantages of the fuel cell are;

(1) High initial costs of the system(catalyst and accessories)

(2) Large weight and volume of gas fuel storage system

(3) Liquifaction of hydrogen takes 30% of the stored energy

(4) High price for clean hydrogen

(5) Need to continuously clean alkaline cells since they suffer from carbon dioxide degradation.

Table 1.2: Demonstrated Efficiencies of Direct Energy Converters. [31]

Energy Converter	%Efficiency
Thermoelectric	10
Thermionic	22
Photovoltaic	18
Magnetohydrodynamics	60
Low Temperature Fuel Cell	60
High Temperature Fuel Cell	60
Gas Turbines	30
Internal Combustion Engines	30
Diesel Engines	30

(6) Low specific power of fuel cells. The specific power of fuel cells is only 1/5 th that of a typical combustion engine.

(7) Precious metal catalysts as used in the preparation of the electrode suffer from sulfur deactivation.

1.3 Types of Fuel Cells.

One type of classification of the fuel cell is given by both Geoffrey[4] and Liebhafsky[5]. Table 1.3 shows this classification where a broad distinction is made between direct and regenerative fuel cells.

The classification based on the type of electrolyte is most relevant and is also shown on table 1.4. In fuel cells where the connecting electrolyte to the electrode is an ion-conducting solid oxide, the operating temperature is 1000°C. For carbon melt electrolyte the temperature is 600°C and for phosphoric acid the temperature is 200°C. Other electrolytes are solid-ion permeable membranes like Nafion and alkylhydroxides.

Hydrogen-Oxygen Fuel Cell

In a hydrogen - oxygen fuel cell, the electrolyte could be a basic solution such as KOH, NaOH, an acid or a molten substance. The hydrogen electrode is either platinum or nickel and the oxygen electrode is silver. In this system, hydrogen is the fuel and oxygen or air is the oxidant. Water is the product from the combustion reaction.

Table 1.3: Classification of Fuel Cells. [31]

FUEL CELLS

DIRECT			INDIRECT		REGENERATIVE
Low Temperature	Intermediate Temperature	High Temperature	Reformer	Biochemical	
1. H_2/O_2	1. H_2/O_2	1. H_2/O_2	1. Natural Gas	1. Glucose	1. Thermal
2. Organic Compounds - oxygen	2. CO/O_2	2. CO/O_2	2. Naphtha	2. Carbohydrate	2. Electrical
3. Nitrogeneous compounds - oxygen or hydrogen peroxide	3. NH_3/O_2		3. Methanol	3. Urea	3. Photochemical
4. H_2/Halogen			4. Ethanol		4. Radiochemical
5. Metal/Oxygen or halogen			5. Coal		
			6. Ammonia		
T < 200 °C	T ~ 200 - 750 °C	T > 750 °C			

Table 1.4: Classification Based on the Electrolyte.[31]

	Alkaline Fuel Cell (AFC)	Phosphoric Acid Fuel Cell (PAFC)	Solid Oxide Fuel Cell (S)FC)	Solid Polymer Electrolyte Fuel Cell (SPEFC)	Molten Carbonate Fuel Cell (MCFC)
Fuel	Pure H	H with CO	H and CO	Pure H	H and CO
Electrolyte	NaOH or KOH Solution	Ortho-Phos - phoric acid	Ion-Conducting Oxide (ZrO with Y O)	Ion-Conducting Membrane (e.g., Naflon	KLiC (Molten)
Operating Temp. C	< 100	< 200	800 - 1000	< 100	~ 650
Electrode Material	Metal or Carbon	Carbon	Cermets or Ceramics	Carbon	Metal-based
Configuration	Monopolar or bipolar	Bipolar	Monopolar or bipolar	Monopolar or bipolar	Bipolar
Stack Material	Polymer	Graphite	Ceramic Tubular Cells and Monolith cells	Graphite Tubular Cells and Monolith Cells	Metal and Polymer
Cost of Materials ($/kW)	15	150	135	500	50

Other fuel cell options include methanol-air, glycol-air, hydrazine-peroxide, ammonia-oxygen, and redox.

Alkaline Electrolyte

A typical Hydrogen-Oxygen fuel cell is the alkaline fuel cell. In this system the electrolyte is KOH or NaOH solution. The diagram of the alkaline fuel cell is shown in figure 1.2. The reactions that take place are shown below.

$H_2(g) + 2OH^-(aq) = 2H_2O(l) + 2e^-$ Anodic Reaction

$\frac{1}{2}O_2(g) + H_2O(l) + 2e^- = 2OH^-(aq)$ Cathodic Reaction

---

$H_2(g) + \frac{1}{2}O_2(g) = H_2O(l)$ Overall Reaction

At the anode, hydrogen is oxidized to form water and simultaneously at the cathode, oxygen is reduced to form the hydroxide. Electrons are released in the process and they flow in the external circuit. Charge is transferred through the electrolyte by the hydroxyl ion.

One advantage of alkaline fuel cells is that the nickel and the silver electrodes used are stable and readily available. The other advantages have been outlined by Thallar [6].

(1) The performance of the cathode is much more improved than the one in acid fuel cells.

(2) The material of construction is low costs.

(3) Corrosion is not as serious as in the acid electrolyte.

However, the disadvantage of the alkaline fuel cell is the formation of

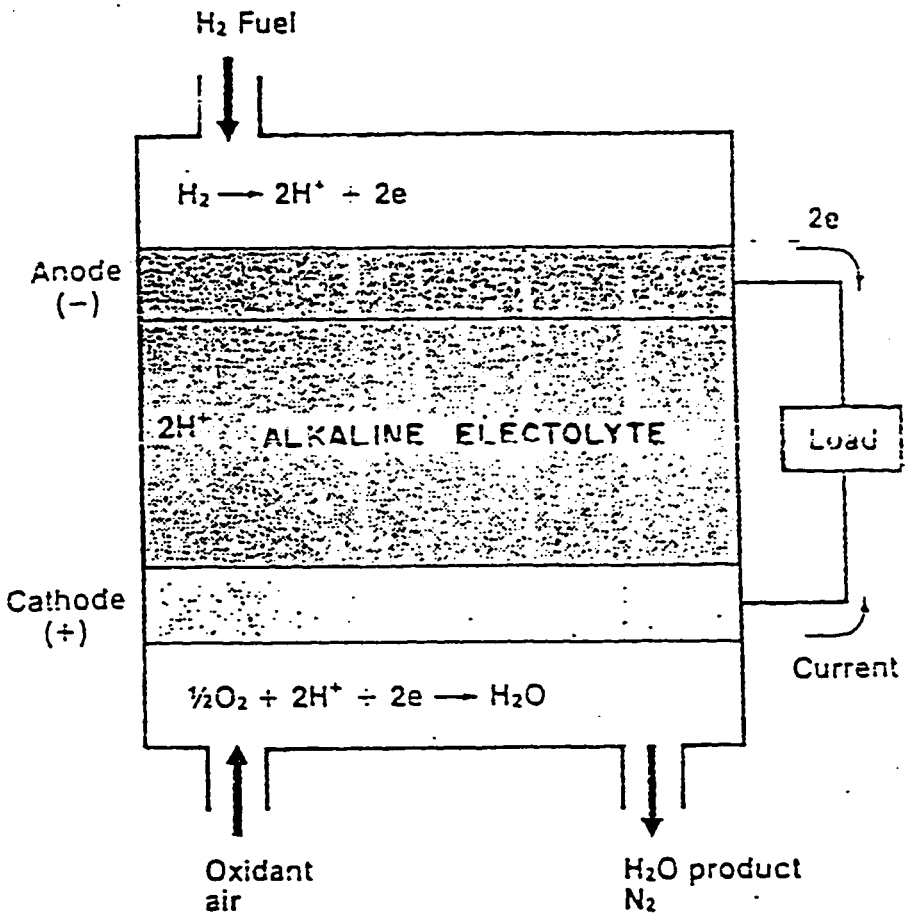

Figure 1.2 : Alkaline Fuel Cell.

carbonate resulting from carbon dioxide present in the fuel.

Other types of hydrogen - oxygen fuel cells include the acid electrolyte and the molten cabonate electrolyte.

1.4 Types of Fuels

Pure hydrogen and pure oxygen are the ideal fuel and oxidizer, respectively. These fuels are generally impracticable due to the high cost and or the weight ratio of the storage tanks relative to the fuel. They are only used in space and undersea applications. A report on the gas fuel cell power market[7] has indicated the successful use of natural gas in fuel cells. In 1986, the United States energy department [8] used methanol in research work on fuel cells. Similar work was also carried out by Gallagher[9] in the United Kingdom and Cowley [10] again from the United States. Coal has been used by Grant et al [11] at a fuel cell plant in Tucson, the U S. Penner [12] has also reported the potential use of biogas as sources of fuel in fuel cells.

1.5 Fuel Cell Applications

Space Application

Fuel cells have been used for a long time in space exploration work by NASA. In 1965, Russel [13] discussed the design of the fuel cell that was used in the Gemini flight. Morril [14] and Sandatede[15] briefly reviewed the advantages that were inherent in the deployment of the fuel cell in the Appollo Space

Flight. Finally, Nuttal [16] described the application of solid polymer electrolyte for space and other high altitude Aerostat programs. A solid polymer electrolyte fuel cell is used in the water electrolysis mode to generate oxygen for spacecraft and submarine life support systems. It is also used in an oxygen concentrator mode so as to generate oxygen for crew in the combat aircraft for heat and power(CHP) generation. In addition, the use of fuel cells for providing power for space radar sensor systems has been given by Boretz [17].

Combined Heat and Power Generation

Warshang [18] reported that although the alkaline fuel cell has been used in specialised applications such as space flight, attention is now focused on using alkaline fuel cells in combined heat and power(CHP) generation. Rastler [19] has demonstrated the use of the phosphoric acid fuel cell for transportation and power generation. The application was divided into three categories, consisting of, low power, medium power and high power applications. The field of low power extends from a few milliwatts to less than 10kW. This covers a wide range of possible applications including remote telephone exchange, radio and television relays, signalling installations and industrial lift trucks. The range for medium power application is 10 to 150kW and is used in generators and farm machinery. High power applications require nominal power higher than 150kW. Possible areas of application are high power generators, railway traction, naval propulsion and power plants.

The use of fuel cells for military applications has been reported by Ching[20] et al, Handley[21] and Newby[22]. They also forcasted that in the early 1990s

cogeneration and combined heat and power plants will begin operation with a 200kw phosphoric acid CHP units. In addition to this, two independent surveys by Sabbioni[23] and Ove[24] have revealed that in Europe, industrial CHP and district heating CHP represent two major forms of fuel cell applications.

1.6 Problems and Limitations of Fuel Cells

Theoretically, there are many possible combinations of electrode materials, fuels, electrolytes and operating conditions for practical fuel cells. However, practical considerations severely limit the choice. Selection of electrolyte immediately imposes a number of constraints. For example, the use of potassium hydroxide requires a temperature range between 50°C and 150°C for optimum operations. Since carbon dioxide reacts with this electrolyte purified air is used. The problem of phosphoric acid electrolyte is that below temperatures of 150°C the conductivity of phosphoric acid is low, but above this range the conductivity increases rapidly. The increase in temperature leads to degradation of the electrolyte.

Most of the limitations involved in fuel cell operations are related to the relatively low temperature of operations. At these temperatures slow electrode reactions are responsible for much of the loss in efficiency. Higher temperature operations with molten salt electrolytes promote electrode reactions, decreasing the need for expensive catalysts. In addition, electrolyte conductivity increases with increasing temperature. Ohmic losses are also reduced. However at high temperature of operation, the electrolyte evaporates and there is a material

failure.

Material and catalyst development are the greatest technical problems. The components must be stable in their respective environments for several hours of operations.

Efforts are concentrated on reducing the expensive platinum content by dispersing it in an inexpensive substrate. Platinum loading has subsequently been reduced from $10mg/cm^2$ to $1mg/cm^2$. Recent developments are therefore aimed towards providing effective non-noble metal catalyst for fuel cell operations.

1.7 Porous Gas-Diffusion Electrodes

Linden[25] has discussed the performance of porous gas diffusion electrodes in alkaline fuel cells. It was stated that low current densities in the range of micro to milliamperes per square centimeters are obtained when gases react on non-porous electrodes at room temperature. Current densities about a thousand times larger are required for the operations of practical fuel cells. To be able to obtain these higher current densities, the electrode structure and the transport processes are of great importance. A good electrode structure must be able to bring gas and the electrolyte together so that the reaction can be easy and rapid. The electrodes must also be able to prevent undesirable mass transfer such as bubbling, floating or weeping. An enlarged porous electrode structure is therefore needed to bring gas and fluid electrolyte together for maximum effectiveness.

A gas diffusion electrode is one which can bring three phases together: gas, electrolyte and the catalyst. Both phosphoric acid and potassium hydroxide fuel cells have electrodes which contain several layers. A backing layer or a gas diffusion layer to serve as a barrier between the electrolyte and the gas phase. This layer is commonly made of a thin sheet of porous teflon with graphite for electrical conduction. In addition, there is a catalyst layer in which the reaction takes place and a conducting grid or perforated metal foil which serves as a support and for conduction of current.

In these electrodes, reactant gases reach the active sites by the process of diffusion. The diffusion in the gas phase is 10^3 times faster than in the liquid phase. Hence high current densities are obtained by using these electrodes as compared to planar electrodes.

Raney Nickel and Raney Silver electrodes

Figure 1.3 shows a picture of the porous gas diffusion electrodes (Raney Nickel for the hydrogen electrode) which has been used in this study. The electrode is specially prepared by DLR of Germany, Stuttgart for the HYSOLAR project in which KFUPM is part of the joint research project group.

These electrodes are essentially Al-Ni and Al-Ag alloys. The Raney alloy catalyst is prepared from a 50-50% mixture of Al and Me (Me is either Ni or Ag) alloy. First, the alloy is treated with potassium hydroxide solution to leach out the aluminium metal. The Raney alloy is then washed with clean water to remove the remaining KOH solution. Following that, the treated alloy is activa-

Figure 1.3 : Picture of the Electrode.

ted in vacuum at 100°C. During this stage, air is let into the system in a stepwise manner. Next the catalyst is mixed with PTFE powder. The composition of the mixture is 92% Me and 8% PTFE for the Raney/Nickel elctrode. This is then milled together in order to decrease the particle size and optimize the particle size distribution. The PTFE is used to bind the catalyst grains and it is usually in the form of wires. Finally, the electrode is obtained by rolling the catalyst paste on a Nickel metal net with a calender.

The Raney electrodes have two types of pores. The macropore is found between the Raney metal grains. These have an average pore size of one micrometer. The other pore size is the micropore system. They are found within the Raney catalyst grains and have average pore sizes of 100nm. The macropore system is filled with the gas while the micropores are filled with the electrolyte.

1.8 Fundamentals of Fuel Cells

1.8.1 Some Relevant Electrode Concepts

1.8.1.1 Double Layer Capacitance.

When an electrode (metal surface) is immersed in an electrolyte, the electronic charge on the metal attracts ions of opposite charge and orient the solvent dipoles. Two layers of charge then exist in the metal and in the electrolyte. This

charge seperation acts like an electric capacitor and it is therefore capable of storing electric charge. It is the establishment of this charge seperation that is known as the electrical double layer of the electrode. Gileadi[26] has presented the Helmholtz parallel-plate capacitor model in order to account for the charge seperation phenomenon. The model is shown in figure 1.4. The author assumed a 'leaky' double layer so that it could be self discharged by electrochemical reactions taking place across the interphase of the electrode-electrolyte boundary. This enabled the author to represent the total impedence of the double layer in the form of a capacitor and a resistor in parallel. He also assumed the initial value of the capacitor to depend on the potential of the cell. With these additional assumptions, he derived a relationship for calculating the double layer capacitance as

$$C_H = \frac{\varepsilon}{4\pi d} \qquad (1)$$

where C_H is the capacitance per unit area of the Helmhotz double layer, ε is the dielectric constant and d is the thickness of the double layer.

Gouy[27] extended the model of Helmhotz and introduced the diffuse component of the double layer. The diffuse component depends not only on the cell potential but also the electrolyte concentration. Figure 1.5 shows the model due to Gouy. The equation for calculating the capacitance of the diffuse component is given by

$$C_d = nF\sqrt{\frac{DC}{2\pi RT}}\cosh(2F\varepsilon / 2RT). \qquad (2)$$

where C_d is the capacitance of the diffuse layer and D is the diffusion coefficient

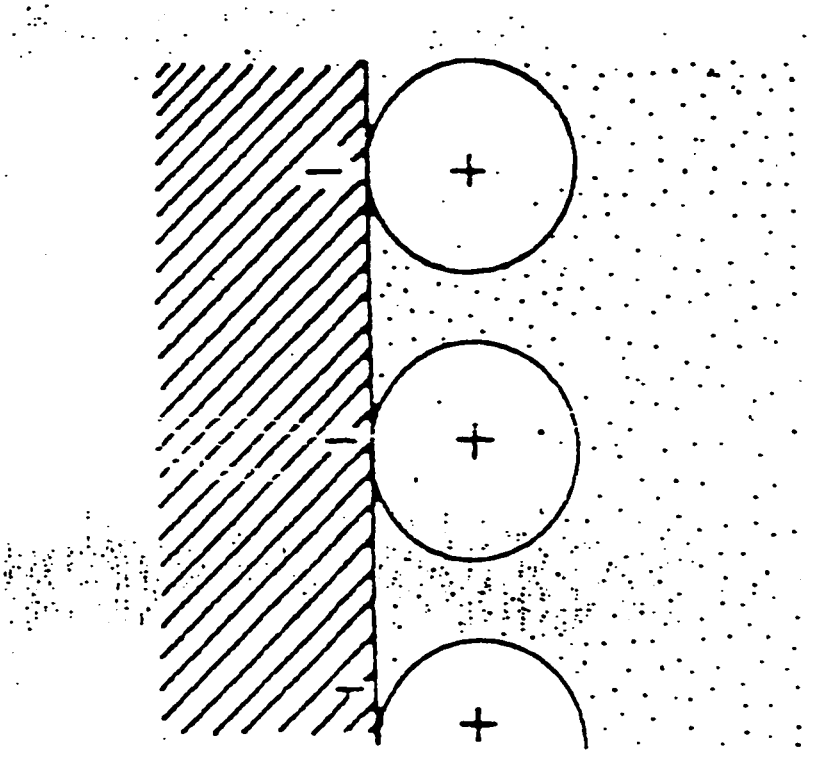

Figure1.4: Diagram of the Electrode Double Layer due to Helmholtz.

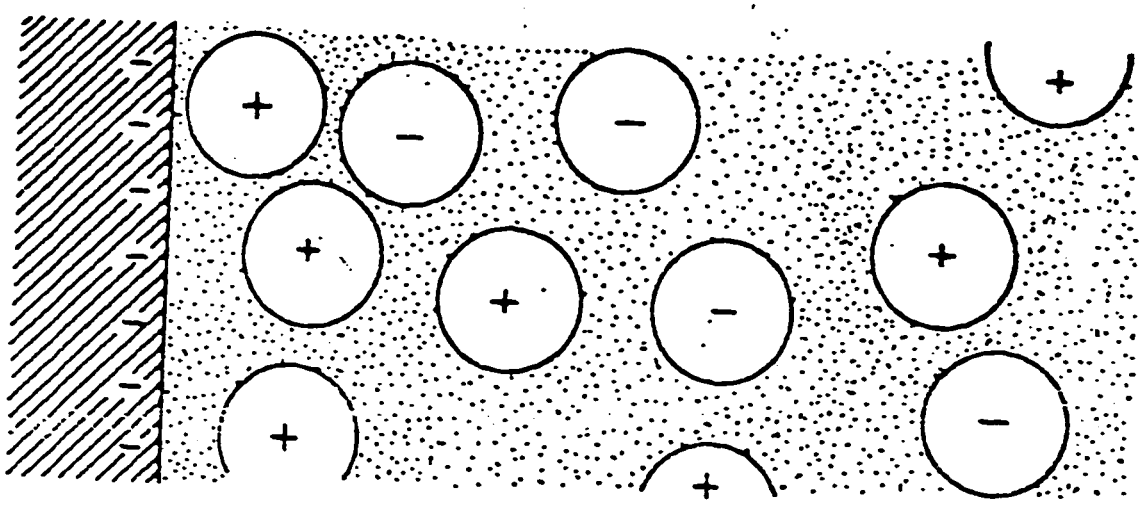

Figure 1.5 : Diagram of the Electrode Double Layer.due to Gouy. [26]

of the ions.

1.8.1.2 Faradaic Current.

During the operation of the cell, current passes through the double layer. Part of this current that passes through the double layer is used to charge the double layer whereas the other part just goes through without doing anything. The fraction of current that is not involved in changing the charge of the double layer capacitor but then passes across the phase boundary by electron transfer is called faradaic current.

1.8.1.3 Exchange Current Density

At equilibrium potential, there are no external flow of current across the fuel cell and so no electrochemical reactions take place at the phase boundary. There exists a static situation on a macroscopic level. However on a molecular scale, a constant exchange of charge carriers (ions or electrons) takes place through the phase boundary. This exchange corresponse to identical anodic and cathodic current densities that compensate each other so that the external current does not flow. The magnitude of these mutually compensating current densities at the equilibrium potential is called the exchange current density. In fact, it is an electrochemical specific rate constant that plays similar roles as the rate constant in ordinary chemical reactions.

Rangarajan[28] emphasised the importance of the exchange current density and mentioned that the magnitude of the exchange current density provides a measure of the electrode performance. In addition, the exchange current density yields information regarding the influence of geometric factor on the size of the

crystallites.

1.8.1.4 Effective Surface Area.

The porous electrode surface provides sites for the electrochemical reactions to occur. However not all the surface area of the electrode is effectively used as reaction sites. The surface area that is effective for participation in electrochemical reactions is known as the effective surface area of the electrode. The values of this parameter are precisely obtained from the measurements of the double layer capacity.

1.8.2 The Thermodynamics of Fuel Cells

The thermodynamics of the fuel cell has been extensively treated by Bokris et al [29].

The basic Gibbs free energy relationship is given by:

$$\Delta G = \Delta H - T\Delta S \qquad (3)$$

Where ΔH is the amount of heat energy from the fuel oxidation. The fuel cell can only convert fuel energy to electricity in an amount equivalent to the Gibb's free energy ΔG. The difference $T\ \Delta S$ is the amount of heat that can be produced in an isothermal, isostatic process which is unrecoverable. Thus the theoretical thermodynamic efficiency is given as:

$$\eta = \frac{\Delta G}{\Delta H} \qquad (4)$$

For example in a hydrogen- oxygen fuel cell system at 25°C, the theoretical

efficiency is approximately 93%.

Internal combustion engines operating between the heat sink temperature T2, and the temperature of the device T1 have an efficiency formulated by Carnot's cycle as

$$\eta = \frac{T_1 - T_2}{T_1} \tag{5}$$

Material of construction and the design are the two considerations that must be made when considering the improvement in the Carnot efficiency.

Under reversible conditions the free energy change ΔG_r of the reaction:

$$H_{2(g)} + \frac{1}{2}O_{2(g)} = H_2O_{(l)} \tag{6}$$

is related to the reversible potential of the cell by

$$\Delta G_R = - n F E_r \tag{7}$$

where ΔE_r is the equilibrium reversible potential of the electrochemical cell and n is the number of electrons taking part in the overall interfacial reaction and F is the Faraday constant. For the activities of the reactants and products in their standard states to be unity then eqn. (7) becomes

$$\Delta G^\circ_r = -nFE^\circ_r \tag{8}$$

where ΔG°_r and E°_r refer to the standard free energy change and standard reversible potential, respectively. Table 1.5 gives some important thermodynamic

Table 1.5 : Thermodynamic Data at 25°C for H_2/O_2 Fuel Cell.[31]

$\Delta G°$(kcal/mol)	-56.69
$\Delta H°$(kcal/mol)	-68.32
n	2
Δn (Change in the mol number)	- 1.5
E_r° (volts)	1.229
$\frac{\partial E_r^\circ}{\partial T}$ (mV/°C)	-0.84
$\frac{\partial E_r^\circ}{\partial \log P}$ (mV)	45
ϵ_i (Efficiency)	0.830

data for the hydrogen- oxygen fuel cell.

At equilibrium, the standard electrode potential E°_r is determined from the standard free energy ΔG°_r of the reaction at 1 atm., 1N solution and 25°C

$$\Delta G^\circ_R = \sum_{j=1}^{i} v_j \Delta G^\circ_{fj} \tag{9}$$

Where ΔG°_{fj} is the standard free energy of formation of species j and v_j is the stoichiometric coefficient of the species j. For product, v_j is positive and for reactants it is negative. The standard potential of the normal hydrogen electrode (NHE) is usually the reference standard electrode and is assigned the value of zero.

In order to determine the reversible potential for conditions other than the standard state, Allen et al[30] employed the chemical potential to obtain

$$\Delta G_R = \sum_{j=1}^{i} v_j \mu_j = \sum_{j=1}^{i} v_j \mu_j^\circ + RT \sum_{j=1}^{i} v_j \ln a_j \tag{10}$$

$$E_r = E_r^\circ - \frac{RT}{nF} \sum_{j=1}^{i} v_j \ln a_j \tag{11}$$

where a_j is the activity of the jth species. Eqn. (11) is known as the Nerst equation. Deviations from the Nerst equation occur for cases of irreversible operation, presence of impurities, multiple reactions, chemisorption on the catalyst surface and formation of reaction intermediates.

For the hydrogen-oxygen fuel cell in an alkaline medium, Tilak et al [31] utilised the fact that the hydroxyl ion concentration is the same at both

electrodes in open circuit and obtained the total cell voltage as

$$E_r = E^\circ_r - \frac{RT}{2F}\ln\frac{a_{H_2O}}{a_{H_2}a_{O_2}^{\frac{1}{2}}} \qquad (12)$$

where E°_r at 25°C is given by the standard reduction potential of oxygen in alkaline media 0.041V minus the standard oxidation of hydrogen in alkaline media(-0.828 V). This gives E to be 1.229V.

1.8.3 Electrokinetics and Modes of Polarization

A complete analysis of the electrokinetics and modes of polarization of fuel cells has been presented by Crow[32].

A potential difference must be maintained between the working and counter electrodes of the cell if an electrochemical process is to occur at finite rate. Current flow is therefore a function of cell voltage. The energy of electrochemical processes is obtained from

$$W = EIt \qquad (13)$$

where W is the energy of the electrochemical process, E is the potential, I is the current and t is the time. For a current efficiency of one, Faraday's law is applicable as given by

$$m = \frac{M}{nF}It \qquad (14)$$

where m is the electrochemically converted mass, M is the molar mass, F is the

Faraday's constant, I the current, t the time and n the charge number of electrode reaction. The chemical reaction rate is obtained by differentiating eqn.(14) with respect to t. Hence we obtain,

$$\frac{dm}{dt} = \frac{M}{nF} I = \text{Rate} \tag{15}$$

The actual working cell potential E is given by

$$E = E_r - \eta_{c,act} - \eta_{a,act} - \eta_{c,conc} - \eta_{a,conc} - IR_i \tag{16}$$

Where η_{act} and η_{conc} are the overpotentials due to activation and concentration, respectively (a is for anode and c is the cathode). IR is the ohmic overpotential, and the rest take their meanings as before.

Bockris et al [33] presented plot of cell potential versus current for a typical fuel cell and this is shown in figure 1.6. When current passes through a fuel cell, the potential of the elctrodes change. This phenomena is called polarization. The overpotential in this case is given by

$$\eta = E_p - E_e \tag{17}$$

where E_p is the polarization potential and E_e is the eqilibrium potential. η is negative for polarization at the cathode and positive for anodic polarization.

An electrode in solution at equilibrium has equal anodic (i_a) and cathodic (i_c) currents. Therefore,

$$i_a = i_c = i_o \tag{18}$$

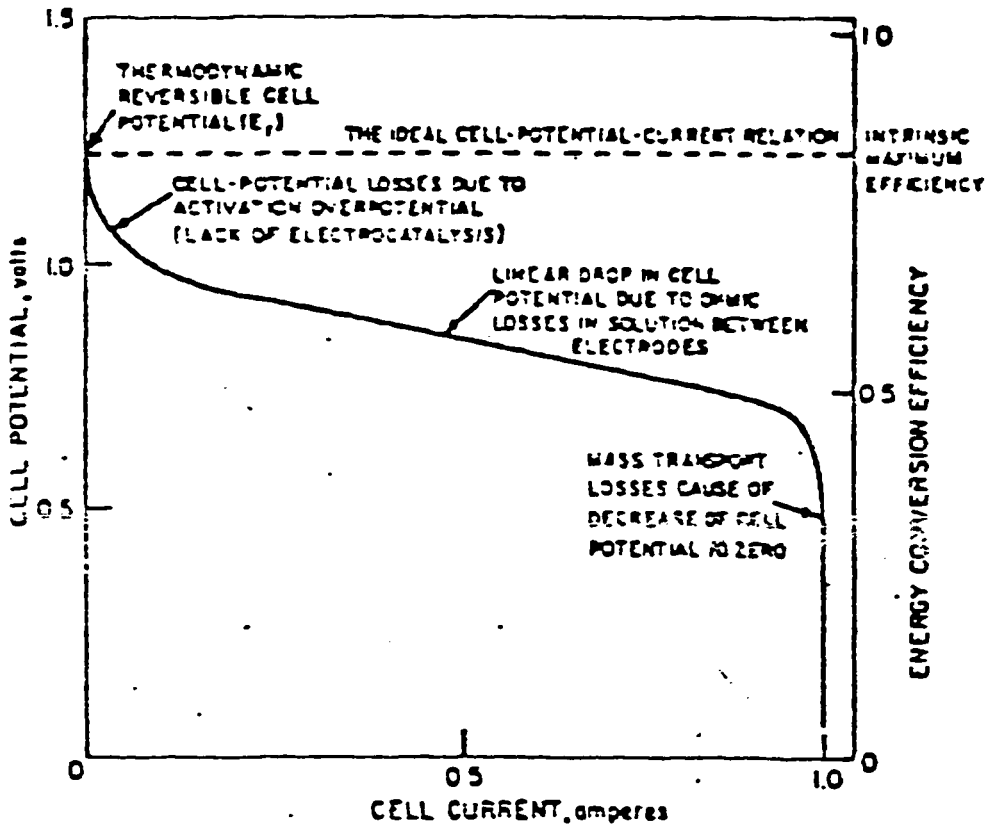

Figure 1.6: Typical Plot of Cell Potential Versus Current.

In eqn. 18, i_o is known as the exchange current density. It is an important kinetic parameter (similar to rate constant in ordinary chemical reactions) of an electron transfer process.

The resultant current through an electrode is given by

$$i = |i_a| - |i_c| \tag{19}$$

This leads to the expression for the Butler-Volmer equation

$$i = i_o\left[\exp(\alpha nF\frac{\eta}{RT}) - \exp\left\{-(1-\alpha)nF\frac{\eta}{RT}\right\}\right] \tag{20}$$

where α is known as the charge transfer coefficient. This value of α establishes the extent to which electric potential changes the energy of activation. At large anodic polarization when η is very positive, i_c is negligible and the current density is given by the anodic partial current density

$$i = i_o\left\{\exp(\alpha nF\frac{\eta}{RT})\right\} \tag{21}$$

Similarly for large cathodic polarization,

$$i = i_o \exp\left\{-(1-\alpha)nF\frac{\eta}{RT}\right\} \tag{22}$$

solving for η from equations 21 and 22 leads to the relationship

$$\eta = a + b \ln i \tag{23}$$

where a and b are constants. Eqn. 23 is known as the Tafel equation. For large enough polarization, the Tafel equation holds, and the situation indicates that

electron transfer is the rate determining step.

Experimental data of η versus ln i can be plotted to give the values of 'a' and 'b'. The exchange current density i_o and α can then be determined.

At high current densities reactants become depleted at the electrodes. This may be due to the fact that electrode processes occur faster than reactants are supplied by diffusion process to the electrodes. Diffusion polarization due to potential changes therefore take place. The current under these circumstances is given by:

$$i = n_j F D_j \frac{C_{j,o} - C_{j,s}}{\delta_d} \qquad (24)$$

where $C_{j,o}$ and $C_{j,s}$ are the concentrations of the species j in the bulk electrolyte and surface of the electrode respectively. δ_d is the thickness of the diffusion layer.

As current is increased, $C_{j,s}$ approaches zero and there is a limiting diffusion current (the maximum current drawn) given by:

$$i_{d,l} = n_j F D_j \frac{C_{j,o}}{\delta_d} \qquad (25)$$

Equation 25 can be expressed in terms of the cell overvoltage as:

$$\eta_d = \frac{RT}{n_j F} \ln \frac{C_{j,s}}{C_{j,o}}$$

$$= \frac{RT}{n_j F} \ln\{1 - \frac{i}{i_{d,l}}\} \qquad (26)$$

1.9 Objectives

The determination of the electrode double layer capacity of porous bodies will lead to proper interpretation of kinetic phenomena. The structure of the electrode is responsible for many of the properties of an electrochemical system. For example, the surface area that is effective for participating in these electrochemical reactions is obtained from the determination of the double layer. By comparing experimental values of the specific surface area with that obtained from BET measurements, Tilak et al[34] concluded that the two values could be significantly different. As discussed earlier, the exchange current density is another parameter of great importance. It is a kinetic parameter playing the same role as the rate constant in ordinary chemical equations. It gives the maximum operating current obtainable as set by the limits of polarisation. Now, with these electrodes it is expected that their characteristics will differ from electrodes reported in the literature primarily due to the methods of preparation. Therefore, it is necessary to determine the double layer capacities and the exchange current densities of these specially prepared electrodes. These parameters will give information of the catalyst surface area and the kinetic behaviour of the reactions. The information obtained through unsteady state techniques will give precise values of the required parameters.

The objectives of this study are:

1. To experimentally determine the

    i. Exchange current densities

ii. Double layer capacities

iii. Activation Energy, and

iv. Surface Roughness Factor

of the hydrogen electrode.

2. To Study the Effects of Temperature on the exchange Current Density and the Double Layer Capacitance by using unsteady state techniques.

These unsteady state techniques include:

a. Exponential relaxation method

b. Triangular sweep

The measurements that are taken to determine the exchange current densities are carried out at different temperature ranges of between 30°C to 65°C. The temperature range is chosen within this range to ensure that no demage is done on the electrode.

The procedure used for the exponential decay is similar to that used by Tilak et al[35]. A modification of the circuit is made so that the results are obtained with ease. The use of direct current (as opposed to alternating current reported in literature), and inexpensive electronic components reduced the cost needed to generate the necessary data.

CHAPTER 2

2.0 Techniques for the measurements of the performance of Fuel Cells

The different types of techniques that are used for determining the performance of fuel cells are illustrated in table 2.1.

The classification is divided into two basic methods, steady state and unsteady state.

2.1 Steady-state techniques

Steady-state techniques are used to characterize electrode performance of fuel cells. This technique is based on the fact that when the electrochemical system is excited all variables reach steady-state after some time. Measurements are therefore taken and analysed using only current and potential relationships.

The information that can be obtained by use of steady state techniques include:

1. The overall kinetic reaction path.
2. Reaction orders and charge transfer coefficients
3. The exchange current density and
4. The limiting current density.

Table 2.1: Techniques for the measurements of the Performance Fuel Cell

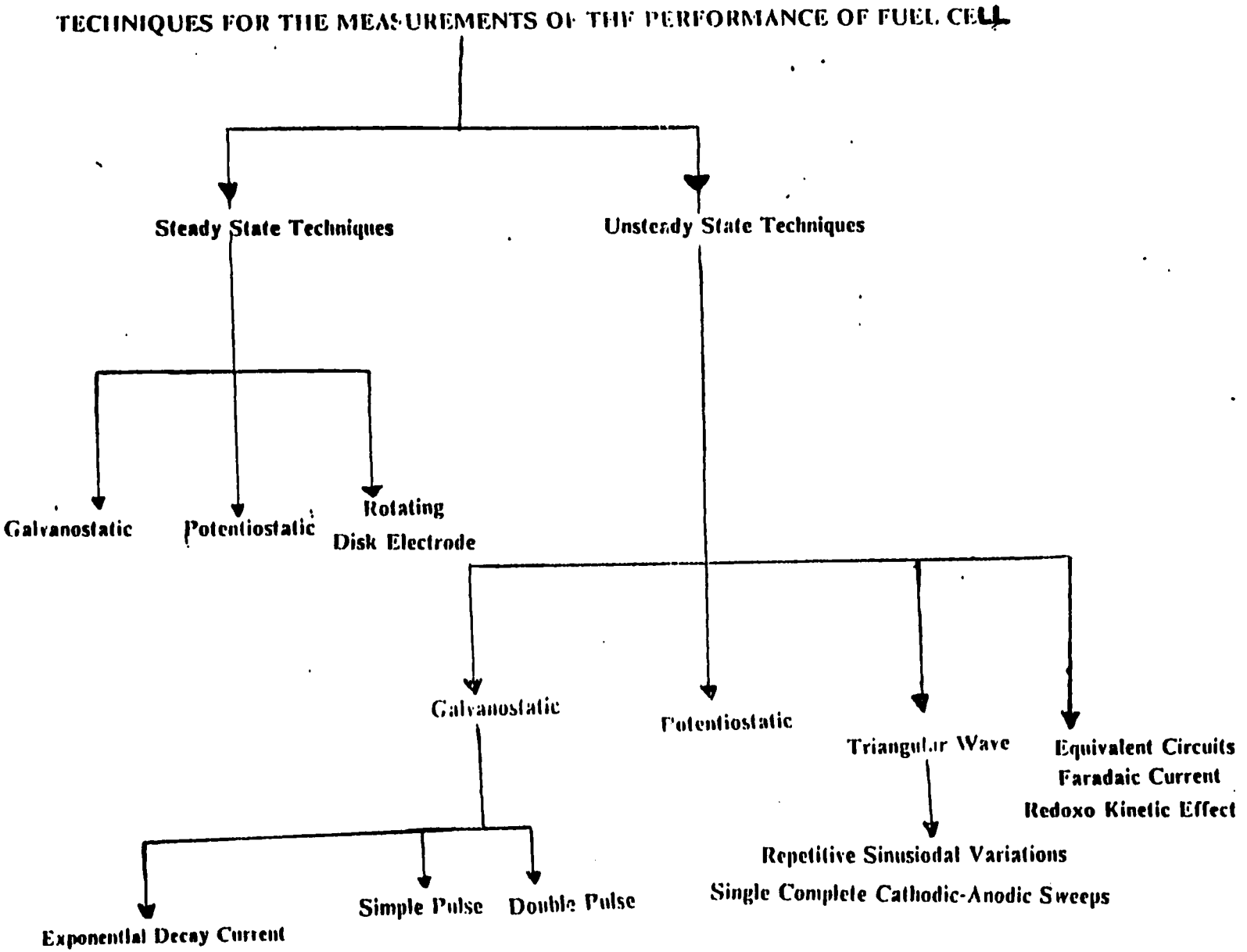

Limitations of the Steady State Methods.

The limitation of the steady-state methods has been discussed by Vetter [36] as follows

1. They do not give information about events prior to and after equilibrium state.
2. They do not give precise values of the parameters under investigation. The values obtained are overall estimates.
3. The time to establish equilibrium in steady state measurements could be long.

In the literature, the steady state methods that have been employed for studying the performance of fuel cell include:

1. Galvanostatic
2. Potentiostatic
3. Rotating disk electrode

2.1.1 Galvanostatic Method

In the galvanostatic method, the current is controlled externally (system at steady-state) and the resulting potential is measured.

Advantages

The major advantage of this method is that it is the only case in chemical kinetics where measurements are made under conditions such that the reaction

is forced to proceed at a chosen rate and so its standard free energy of activation is modified to fit the rate. The other advantage is the simplicity of the method relative to the other techniques.

Disadvantages of Galvanostatic Method

1.It fails for high currents and high cell resistance.

2.It requires the elimination of ohmic potential drop in the test and reference electrodes.

3.It requires rather expensive high voltage power supply.

2.1.2 Potentiostatic Method

In this method the voltage between the test and reference electrodes is kept constant by the passage of current between test and the auxillary electrodes. The resulting current is measured. However, the use of this method had to be delayed until the invention of the potentiostat.

Advantages of the potentiostatic method

1.In the study of some anodic reactions it is necessary to control the region of applied potential otherwise electrode passes to passive region and it will be necessary to reduce the passive film on the electrode before any further studies of reaction are carried out.

2. Passivation leads to a current-potential curve in a way that the current decreases with increasing potential. This is only observed in potentiostatic operation method. Galvanostatic method fails to show this observation.

3. It is easier to obtain reaction rates at constant potential than at constant current. Each determination of rates at constant metal solution potential difference yields a relationship that is directly exploited. However, using galvanostatic method it is necessary to first obtain the entire current relation.

4. This method is valuable in the study of parallel reactions. Coulombic yields of reaction products may be dependent on potential and in this case it is necessary to use controlled potential electrolysis to obtain the relationship between coulombic yields and potential.

5. This is useful in determining the role of mass transfer and its parameters. For example, in the oxidation of ethylene on Pt, it is shown from the observation of current versus time curve in the potentiostatic mode that diffusion of ethylene to the electrode is slow at short times, whereas adsorption of ethylene on the electrode becomes slow at longer times.

2.1.3 Rotating Disk Electrode

In this method, the mechanism of the reaction is controlled completely or partly by mass transfer. The electrode is set in motion with respect to the electrolyte. The main advantage of the technique is that the convective diffusion equations can be readily solved since the mass transfer is controlled.

2.2 Unsteady state techniques

Before discussing the unsteady state methods, first let us find out why it is necessary to use unsteady state methods instead of the steady state methods. The limitations of the steady state techniques had earlier been given.

2.2.1 Why Study Transient?

An inexhaustible list is needed if we attempt to mention all the parameters that can be measured by unsteady state methods but not with steady state methods. Simply put, all parameters that are measured using steady state methods when the system is perturbed during transient will fail to give precise values. To illutrate this further, an example has been chosen. Consider the simple electrochemical reaction given by

$$O + ne \rightarrow R \qquad (27)$$

In this reaction there are atleast five seperate steps that are involved in the conversion of "O" to "R". These steps are:

1. Transport of O from the bulk solution to the interface
2. Adsorption of O on to the surface.
3. Charge transfer at the electrode to form R.
4. Desorption of R from the surface.
5. Transport of R from the interface into the bulk solution.

Now, steps 2-4 are known as the activation process whereas steps 1 and 5 are known as the mass transfer process. In order to get the rate of the overall reaction, the sequential rates of the individual steps must be

taken. Therefore if the system is perturbed under unsteady state conditions, the individual rates will depend on time. The precise values for the rates of these steps are analysed based on unsteady state conditions.

To further illustrate the importance of unsteady state techniques consider again the kinetics of the reaction considered already. Suppose that a potentiostatic control is exerted on the system. Then at the surface, the rate of the reaction is given by

$$i/nFA = k_f C_o (x=0) \tag{28}$$

where k_r is the potential dependent constant and $C_o(x=o)$ is the concentration of O at the interface. At time $t=0$, the rate equation can be written as

$$i/nFA_{t=0} = k_f C_o \tag{29}$$

This equation is valid because the k_r responds spontaneously to the imposed potential while the concentration does not respond. The value of k_r could then be easily obtained if the rate at $t=0$ is known. However, at longer times the effects of mass transfer set in and the kinetics will have to be formulated to take the time dependence of the diffusion steps into consideration. The addition of the time variable enables a greater manipulation of the results.

In addition to the cases considered in this example, when adsorption of intermediate electroactive species take place, the extent of coverage is

only determined by unsteady state methods. To summarise, the precise values of the parameters such as the electrochemical rate constant, the diffusion coefficients and the adsorption coverage can only be determined by unsteady state methods. Some of the added advantages of using unsteady state methods are:

1. Used as a check on parameters obtained by steady state methods
2. Used in the study of faster reactions.

The following are the types of transient techniques

2.2.2 Galvanostatic Method

In the galvanostatic transient, the current is controlled externally and the resulting potential is measured as a function of time.

2.2.2.1. Simple Pulse

The technique of simple pulse consists of passing small impulses of current on the system and measuring the potential as a function of time.

Uses of the simple pulse technique

1. To analytically determine the bulk concentration.
2. To conveniently determine the diffusion coefficient if it is unknown.
3. To obtain charging curves from which information on intermediate reaction is obtained.
4. To obtain charge transfer coefficient and rate constant for irreversible reactions.
5. To study electrochemical reaction preceded by a fast reaction step.

The transient times under simple pulse conditions has been given by Nicholson[36]

$$\tau^{1/2} = \frac{\pi^{1/2} n F D^{1/2} C}{2i} \qquad (30)$$

where τ is the transition time(i.e. the period of time between the commencement of electroreduction and the sudden change in potential). A plot of $1/\tau^{1/2}$ versus i gives a straight line from which the diffusion coefficient can be obtained. This is true for the case of equal potential. However, in situations where there are two componenets the electroactive species occur at different potential. In this case, the transition times are given by :

$$(\tau_i + \tau_2)^{\frac{1}{2}} - \tau_i^{\frac{1}{2}} = \frac{\pi^{\frac{1}{2}} n F D^{\frac{1}{2}}}{2i} \qquad (31)$$

where n, D and C refer to the second electroactive component, and a plot of $1/i\{(\tau_1 + \tau_2)^{1/2} - \tau_1^{1}/2\}$ versus i gives a straight which can be used to determine the diffusion coefficient D.

2.2.2.2 The Exponential Relaxation Technique

Background

The model that was earlier used to calculate the distribution of current and potential in porous electrodes was that due to Daniel'-Bek[37]. The author used a simple model of a one-dimensional pore which is mathematically equivalent to that of Wiesselberg et al [38] and Waber [39] when they studied transmission lines(the 'Telegrapher's equation'). Daniel'-Bek treated the model as identical

distinct, non-interconnected pores. The distribution of electrolyte and electrode resistance are uniform throughout the entire length of the pore. The author also treated both linear and exponential cases of current. Frumkin[40] introduced average potentials to account for the neglect of the curvature of the equipotential surfaces within the pores.

In this technique, an exponential decaying current of the form

$$i(t) = \Delta i \exp(-\frac{t}{\tau}) \tag{32}$$

is employed to stimulate the electrode. Δi is the step change of current and τ is the time constant associated with the exponential input function. The response of voltage versus time is measured. This technique appears to be unique for two reasons:

1. The simple pulse galvanostatic method(earlier described) can be viewed as a special case of the exponential technique.
2. Both the double pulse and the alternating current(a.c) techniques can be deduced from the exponential relaxation technique. The reason is that τ in the exponential method plays a similar role to the frequency in the a.c techniques. The added advantages of this technique include :

a. The simplicity as regards the experimental generation of the input profile and the easy theoretical treatment of the results. Linearization is done taking advantage of the exponential.

b. The overpotential is always brought back to its equilibrium value. This is is due to the unique way of pertubating the system.

c. The maximum in the response potential versus time can be qualitatively explained by the fact that initially the potential has a tendency to

increase but the current decreases with time hence the observed maximum.

Theoretical considerations

In previous studies by Ksenzhek [41] and Winsel[42] the authors used an approach that was based on a heterogeneous sources and sinks in order to quatitatively treat the porous structure. However, a homogeneous phase was developed in the literature to replace the heterogeneous interconnected multiphase system. Figure 2.1 shows the representation of the porous structure.

The assumptions of the model

1. Each single pore has a uniform cross- section and they are filled with eletrolyte. The porous structure is thus visualised as a homogeneous medium. It is assumed to be isotropic in behaviour.
2. Convective diffusion and migration are not considered.
3. Potential(current) distribution is given by a simple equation with the insured hypothesis that the solution and matrix conductivity are constant.
4. Only small pertubations from equilibrium conditions are examined using a linear current versus potential realtionship. (The porous electrode is then viewed as equivalent to a transmission line of finite length with electrolyte resistance in series shunted by a parallel combination of double layer and Faradaic impedences).

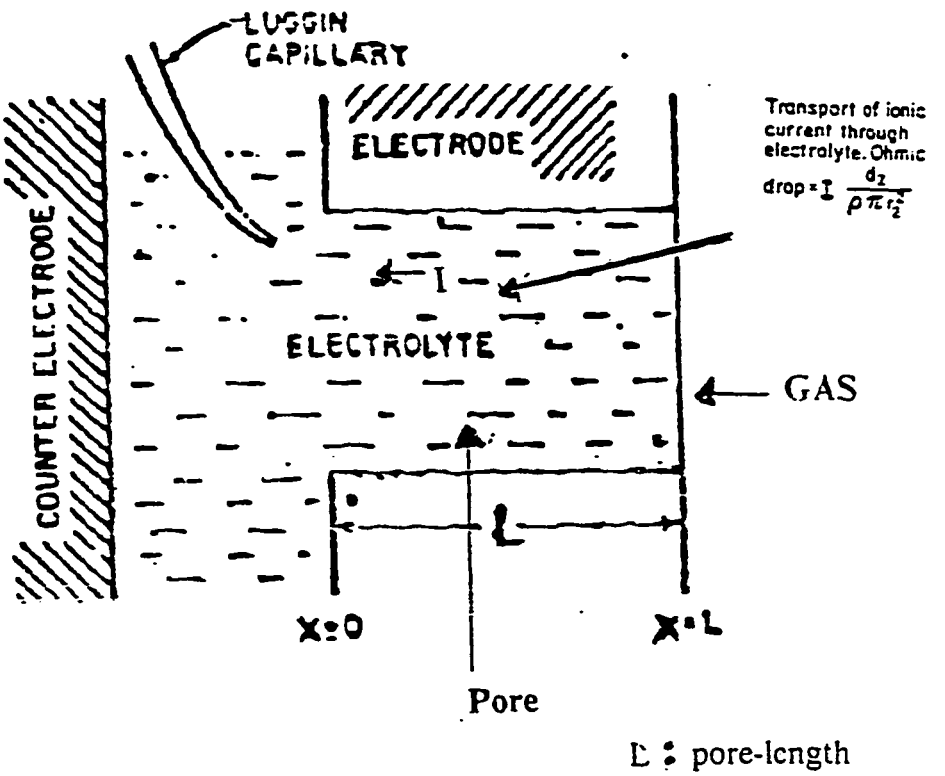

Figure 2.1: Diagrammatic Representation of the Electrode Struture.

Mathematical Formulation of the problem

The formulation of the problem is made by considering the diagram of the electrode structure as shown in figure 2.1.A detailed derivation of the problem is included in appendix C. We define a dimensionless distance as $\zeta = x/L$ then for the initial condition it is assumed that at the start of passing current the potential is zero therefore,

I. C.

$$\eta(0,0) = 0 \tag{33}$$

Boundary conditions:

B.C.1

At the gas side of the electrode, the change in potential is zero. In otherwords there is a constant potential in the neighbourhood of the gas electrode interface. This is analogous to the heat transfer at the an impermeable boundary.

$$\frac{\partial \eta}{\partial \zeta}(0,t) = 0 \tag{34}$$

B.C.2

At this boundary, the current is transported by the electrolyte to the surface of the electrode therefore,

$$\frac{\partial \eta}{\partial \zeta}(1,t) = -R_o i(t) \tag{35}$$

where $i(t) = \Delta i \exp(-\frac{t}{\tau})$ and R_o is the resistance of the electrolyte per unit length of the pores.

At any instant, the impressed current is a sum of the double layer charging and the Faradaic currents. In terms of overpotential it is given as (refer to Appendix C, part A for the missing steps):

$$\frac{\partial^2\eta}{\partial\zeta^2} - \alpha\eta - \beta\frac{\partial\eta}{dt} = 0 \qquad (36)$$

where $\alpha = R_o\frac{Fi_oSL}{RT} = \frac{R_o}{R_t}$. This is the ratio of electrolyte resistance in the pores to the charge transfer resistance .

$\beta = R_oC_T$. This is also the time constant of the double charging and C_T is the total capacitance of the double layer.

The solution to the system of differential equations is(refer to appendix C for detailed solution)

$$\eta = -R_oi(t)\left\{\left[\exp\frac{(-t(B-\frac{1}{\tau}))-1}{\beta(B-\frac{1}{\tau})}\right] + \left[\frac{2}{\beta}\sum_{n=1}^{\infty}\frac{(-1)^n\cos n\pi(1-\zeta)\,(\exp(t(A_1-\frac{1}{\tau}))-1)}{(A_1-\frac{1}{\tau})}\right]\right\} \qquad (37)$$

where

$$A_1 = \frac{n^2\pi^2+\alpha}{\beta}$$

$$B = \frac{\alpha}{\beta}$$

Differentiation of equation(37) with respect to t gives a maximum η_m and t_m.

These values will be the experimentally accessible quantities. The expression for

$\eta_m (\zeta=0)$ is given by:

$$\frac{\eta_m}{i\Delta\tau} = \frac{1}{C_T} \exp(-\alpha\frac{t_m}{\beta})\, \theta_3(x) \left[\exp(-\pi_2\frac{t_m}{\beta})\right] \qquad (38)$$

where $\theta_3(x)$ is Jacobian 0 function is defined as

$\sum_{n=0}^{\infty} \zeta_n X_n^2$ ($\zeta_n = 1$ for $n=0$, $\zeta_n = 2$ for $n > 0$).

Simplifications:

1. $\beta \rightarrow 0$.

This situation corresponds to a shift in control from R_o (electrolyte resistance in the pores) to R_T (charge transfer resistance) and double layer capacitance C_T.

$$\frac{\eta_m}{\Delta i\tau} = \frac{1}{C_T} \exp(-\alpha\frac{t_m}{\beta}) \qquad (39)$$

Several curves of η versus t will be obtained from which η_m and t_m will be used to plot a straight line of $\ln\frac{\eta_m}{\Delta i\tau}$ versus t_m. The slope will be $\frac{\alpha}{\beta} = \frac{1}{R_T C_T}$ and the intercept will be $\frac{1}{C_T}$. Therefore, the double layer capacitance and the exchange current density can be obtained. The slope when $\beta \rightarrow 0$, will yield a value of the charge transfer resistance R_T from which the exchange current density i_o can be obtained.

2. $\beta \rightarrow$ infinity.

This situation now corresponds to a shift in control from R_T (charge transfer

resistance) to R_T (electrolyte resistance in the pores) and double layer capacitance C_T.

The relevant condition that holds is

$$\frac{\eta_m}{\Delta i\tau} = \sqrt{\frac{(R_o}{\pi t_m C_m}}) \exp(-\alpha\frac{t_m}{\beta}) \qquad (40)$$

Thus a plot of $\ln\left[\eta_m t_m^{\frac{1}{2}} \frac{\pi^{\frac{1}{2}}}{\Delta i\tau}\right]$ versus t_m will yield a straight line of intercept $\sqrt{\frac{R_o}{C_T}}$ and slope $\frac{\alpha}{\beta}$.

The explanation for the origin of the maximum is as follows: Initially the potential η increases because of the addition of the input current. However the input current decreases exponentially and the effect tends to decrease the cell potential. Since the change in the direction is gradual, it leads to the formation of a maximum.

2.2.2.3 Triangular Wave

The response of the potential with time in the absence of Faradaic current is given by Posey[43].

$$\frac{\eta(\varepsilon,t)}{iR_o} = \frac{t_o}{\tau} + \frac{2}{\pi^2}\sum_{k=1}^{\infty}\frac{(-1)^k}{k^2}\cos[\pi k(1.-\varepsilon)]\left[\exp(\frac{\pi^2k^2t_o}{\tau}) - 1.\right]\exp(\frac{-\pi^2k^2t}{\tau}) \qquad (41)$$

where t_o is the initial time and t is the time at any period of the transient. The relaxation transients will be described for the case of $t > t_o$. This is the period during the transient. In this case, the current wave may expressed as

$$i(t) = \mu t \quad (0 <= t < \frac{T}{2}) \tag{42}$$

$$i(t) = \mu(T-t) \quad (\frac{T}{2} <= t < T) \tag{43}$$

where $\mu(\frac{amp}{s})$ is the constant rate of change of applied current. T is the period of the triangular wave. At low frequency i.e $T >> t$ equation (44) gives the maximum potential excursion.

$$\frac{\eta(0,\frac{T}{2})}{i(\frac{T}{2})\, R_o} = \frac{T}{4\tau} \tag{44}$$

Hence, C_T can be estimated since the relationship $\tau = R_o C_T$ is valid.

Macdonald [44] has presented the equation expressing the linearized (faradaic) current - potential relationship and when the reaction is controlled exclusively by the charge transfer at the surface. This is given by,

$$i(t) = C_T \frac{d\eta}{dt} + i_o n F \frac{\eta}{RT} \tag{45}$$

The exchange current density can then be determined with the values of the double layer capacitance.

Determination of the Activation Energy of the Electrode Process

Similar to chemical reactions that are not influenced by the potential, the magnitude of the exchange current density characterizes the rate of the electrode process that takes place by charge transfer. In this instance, the exchange

current densities at the anode and cathode respectively are given by Erdey-Gruz[45].

$$i_o = n F k_1 C_o \exp\left[\frac{-U_a^o - \alpha nF\eta}{RT}\right] = n F K_2 C_o \exp\left[\frac{-U_c^o + (1-\alpha)nF\eta}{RT}\right] \quad (46)$$

where k_1 and k_2 are constants corresponding to the pre-exponential factors in the collision theory and U_a, U_c refer to the activation energies for the anode and the cathode respectively.

Combining all the constants of equation (46) including concentrations regarded also as constants, we obtain,

$$i_o = K_a \exp\left[\frac{-U_a^o - \alpha nF\eta}{RT}\right] = K_c \exp\left[\frac{-U_c^o + (1-\alpha)nF\eta}{RT}\right] \quad (47)$$

Now, taking the logarithms of equation (47)

$$\ln i_o = \ln K_a - \frac{U_a^o - \alpha nF\eta}{RT} = \ln K_c - \frac{U_c^o + (1-\alpha)nF\eta}{RT} \quad (48)$$

The equilibrium potential is related to the free energy change associated with the process by

$$n F \eta_e = -\Delta G. \quad (49)$$

$U_a^o - \alpha nF\eta_e$ and $U_c^o + (1-\alpha)nF\eta_e$ are the equilibrium activation energies at the anode and cathode respectively. Consequently,

$$U_a^o - \alpha n\eta_e = U_c^o + (1-\alpha)nF\eta_e \quad (50)$$

Substituting eqn.(50) into eqn. (48) gives,

$$\ln i_o = K - \frac{E_a}{RT} \tag{51}$$

where E_a is the activation energy. Hence a plot of the ln i_o versus $\frac{1}{T}$ will give a straight line. The activation energy will then be obtained from the slope of the plot.

2.2.3 Potentiostatic Method

In the potentiostatic method, the potential of the test electrode is controlled externally and the time variation of the resulting current density from a step-like change in the potential is studied.

For example, a typical potentiostatic transient of the reaction

$$R \rightarrow P + ne_o^- \tag{52}$$

has a rate equation given by:

$$i = i_o\left[\frac{C_R}{C_R^o}\exp(\alpha\eta\frac{F}{RT}) - \frac{C_p}{C_p^o}\exp\left\{-(1-\alpha)\eta\frac{F}{RT}\right\}\right] \tag{53}$$

where C^o corresponse to the initial concentration and C the concentration at any time. R and P refer to reactants and products respectively.

The current decreases with time since C_R decreases due to its consumption while C_p increases. If x is the distance from the planar electrode then, the boundary conditions for the diffusion of reactants to and products away from the electrode are:

$$C_R = C_R^o \text{ and } C_P = C_P^o \quad \text{at } x > = 0, \text{ and } t=0 \tag{53}$$

$$C_R = C_R^o \text{ and } C_P = C_P^o \quad \text{at } x=\infty \text{ and } t > =0 \tag{54}$$

$$i = n F D_R\{\frac{dC_R}{dx}\} \text{ at } x=0 \text{ and } t > 0 \tag{55}$$

$$D_R\{\frac{dC_R}{dx}\} + D_P\{\frac{dC_P}{dx}\} = 0 \text{ at } x = 0 \text{ and } t > 0 \tag{56}$$

The solution of this diffusion equation with the boundary conditions is given by both Gerisher [46] and Gerisher et al [47] as

$$i = i_o\left[\exp(\alpha\eta\frac{F}{RT}) - \exp\left\{-(1-\alpha)\eta\frac{F}{RT}\right\}\right]\left[\exp(\lambda^2 t)\operatorname{erfc}(\lambda t^{\frac{1}{2}})\right] \tag{57}$$

where

$$\lambda = \frac{i_o}{n F}\left[\frac{\exp(\alpha\eta F/RT)}{C_R^o D_R^{1/2}} + \frac{\exp-(1-\alpha)\eta F/RT}{C_P^o D_P^{1/2}}\right] \tag{58}$$

Simplification of eqn.(58) is proceeded as follows:

1. No mass transfer limitation $\lambda = 0$

   This implies, $\exp(\lambda^2 t)\operatorname{erfc}(\lambda t^{\frac{1}{2}}) = 1$, and i is expressed by the equation for activation control. This product decreases with increasing t which shows the effect of mass transfer on the reaction rate. At t = 0 there are no mass transfer effects. As $t \to \infty$ the product of the last two terms and consequently the current density tend to zero.

2. The other simplification that can be made is when the mass transfer is effective. In this case a plot of i versus $t^{\frac{1}{2}}$ is linear. A curve of i

versus η can be obtained from an extrapolated i value of the i versus $t^{\frac{1}{2}}$ plot to t = 0, from which i_o and α can then be obtained.

2.2.4 Slow Triangular Sweep Method

For the case of the slow triangular sweep method the potential of the electrode is controlled externally and varied linearly with time from a starting potential E_i to a final potential E_f and the potential is reversed from E_f to E_i This is related to polarography and involves a continuous(as opposed to a stepwise) change in the electrode potential.

The two methods used are single and multistep. A large number of labels are used to describe the methods depending on whether the method involves single or repetitive sweeps or whether the actual electrode potential is stabilized with a three electrode potentiostatic circuit arrangement. Based on this, the potential-time graphs applied are;

1. Repetitive sinusoidal variations
2. Single linear anodic ar cathodic sweeps
3. Single complete cathodic-anodic sweeps
4. Repetitive cycle saw-tooth variations etc.

Now, depending on only the sweep rates, three types of sweep methods can be identified.

1. Low sweep rates: These are sweep rates that are in agreement with the current-potential relationships obtained in galvanostatic or potentiostatic

method.

2. Intermediates sweep rate: This sweep rate is a departure from the steady state and so,
   a. there is diffusion to and from electrode
   b. possible slow adsorption-desorption equilibrium all set in.
3. High sweep rates: In this method the current measured are used to charge the double layer and for the processes of adsorption or desorption of reactants or intermediates to or from the electrode in a charge transfer step.

Advantages of the sweep method

1. Sweep rates could be low enough for quasi steady state behaviour but fast enough to eliminate interference of the reactions by the diffusion of impurities to the electrodes.
2. Apparatus is quite easily set up and current versus potential is directly obtained.
3. Useful for the analytical determination of the reactant concentration since i_m is in linear variation with the concentration of reactants.
4. The change of form of the polarogram with sweep rate, concentration and temperature can under favourable cases provide simple diagonostic information about the mechanism of the reaction.

Disadvantages of the sweep method

1. There is the need to establish the consistency of the kinetic parameters over a range of sweep rates. The rate determining step may change in the

intermediate region. The Tafel slope in the intermediate sweep region is 35% higher than the slow rates.

2.On set of convection, sweep rates are limited at one end to a few millivolts per second. At the other end, double layer current limits it to a few volts/sec.

3.Difficulty in accurately impressing the sweep rate on the interfacial potential.

4.The mathematical treatment is difficult even for simple cases of linear sweep because of the nature of the boundary conditions.

CHAPTER 3

3.0 Literature Review

This chapter will present a review of the literature on research activities related to the use of transient techniques to determine the performance of the electrodes of fuel cells. The first part of the presentation will discuss a general review of some important studies on transient methods applied in electrochemical studies. In the second part, the review will concentrate on the specific techniques applied to the studies of transient in porous electrodes. More importantly, the introduction of the exponentially decay current technique to be used in this research work will be focussed. In all the review works, the problems and the limitations confronting these earlier techniques will be highlighted.

3.1 General Review

Linear and Triangular Scanning Methods.

Randles [48] was the first to analyse the case of a single reversible electron transfer reaction involving soluble species at planar electrodes for cases of single linear sweep. The simplest case the author considered was the reaction,

$$O + ne^- \rightarrow R. \qquad (59)$$

The author made the assumption that when the potential is stepped to a value near that of equilibrium, the surface concentration of O in the reaction equation

could not be zero. Based on that, he analysed the reversible case of rxn (58) and presented the current/time profiles as given in equation (59)

$$i = n F A D_R^{1/2} \frac{C_o}{(1+k0)\pi^{1/2}t^{1/2}}. \qquad (60)$$

The author then compared his equation to the well known Cottrel[49] equation which is given by

$$i = \frac{n F A D_R^{1/2} C_o}{\theta\pi^{1/2}t^{1/2}}. \qquad (61)$$

He found that the predicted current varied inversely with the square root of the time as shown earlier by Cottrel. However, his equation revealed that apart from the current and time realtionships, the current profile also depended on the step potential θ. Delahay [50] reviewed the work of Randles and added the irreversible case to the studies. The author expanded his work to include the more general case of the situation where the kinetics of the electron exchange at the surface exerted an influence on the reaction analysed already. Several schemes were presented and the methods of handling the boundary-value problems that often arise from the mathematical formulation were treated and could now be handled.

In 1964, Nicholson and Shain[51] used both single and cyclic triangular wave scanning methods to analyse first-order chemical reactions. They discussed cases of reactions preceding, succeeding and parallel to reversible and irreversible charge transfers. In addition, the authors treated electron transfer-chemical reaction-electron transfer(e.c.e) mechanism. In their study, the kinetic

chemical reaction-electron transfer(e.c.e) mechanism. In their study, the kinetic information to be analysed is obtained from the scanning curves where the principal sources for the analysis was based on the observations from current-potentials plots, the change in the number of peaks, and the peak potential-current variation with sweep rates and concentrations. The authors also expanded their work to give a comprehensive treatment of homogeneous first order chemical reactions coupled with an electron transfer step. They adapted the approach of Gokhshtein [52] and presented numerical procedures for solving the integral equations. The numerical approach was general and could be easily applied to many single and triangular wave scanning techniques. However, cyclic scans are undesirable in studying electrokinetics because of the problem of switching potential . Switching potentials are only usefully employed to study chemical kinetic complications in a reaction scheme from the variation of the ratio of anodic to cathodic peak heights with sweep rates.

Servient and Vianello[53] provided a useful general treatment of chemical polarisation during a single linear sweep. A theory was presented to calculate the the current/time curves for linearly varying potential. The reaction scheme used is as follows:

(62)

$$I \underset{k_b}{\overset{k_f}{\rightleftharpoons}} A \overset{ne}{\rightleftharpoons} B,$$

To enable the authors obtain meaningful results, the following assumptions were made:

1. The mass transfer takes place only by semi-infinite linear diffusion.
2. The electron transfer is fast so that Nerst equation is obeyed.
3. The reaction is first order and the double layer capacitance is negligible.

The authors also discussed cases of the reaction being controlled by diffusion of currents, kinetic currents(general cases) and pure kinetic controlled currents. They plotted graphs (shown in figure(3.1)) to discuss the various controlled zones. The authors also remarked that it was possible to vary the potential sweep rate within a wide range so that a situation can be reached where the current/potential curves will be independent of the chemical reaction. In this case, the authors concluded that the equilibrium constant of the reaction is obtained independently from the rate constants. However, the practical limitation of the scheme is that when the capacity current becomes greater than the faradaic currents, the derived equations will need to be considerably modified.

Will and Knor[54] contributed to the scanning techniques and used linear sweep methods to study the various processes involving discharge with adsorption of the radical species. However, it was Conway et al [55] who first gave the theoretical relationship to this study. They concluded their study on adsorbed intermediates with a surface charge transfer reaction. They then suggested the use of single sweep method for studying adsorption of radicals because the opposite changes of the sweep current made the variation of the ion

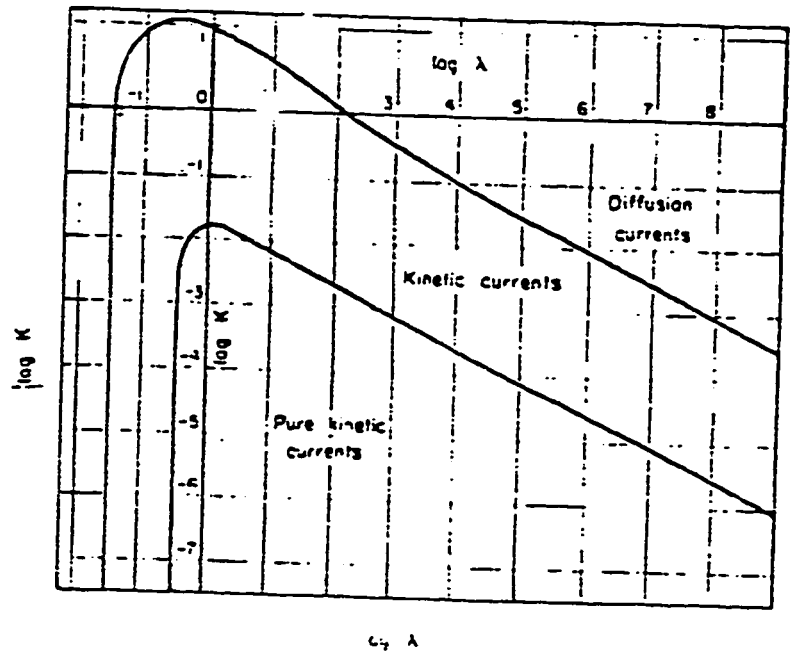

Figure 3.1: Diagram Defining the Various Zones Controlling the Reaction Process.

$$\lambda = \frac{R\,T\,K}{n\Gamma v}$$

: K : Equlibrium Constant

concentration much smaller so that diffusion overvoltage was suppressed. Finally, Hale and Greef (56) extended the treatment by removing the restrictive assumption that the energy of activation is independent of the extent of coverage. In addition, they simultaneously accounted for the interactions between adsorbed species and the non-uniformity of the absorbate. They derived equations for cases of pseudo-equilibrium and irreversibility with negligible back reaction. The authors presented the analysis of the experimental capacitance/voltage curves and noted that it was necessary to incorporate an arbitrary function of the coverage into the activation energy in order to be able to fit experimental data with that from theory. The authors then concluded that, the derived equations were suitable for the triangular sweep method because the rate of the potential change could be conveniently varied and be observed experimentally so that the parameters are easily calculated.

3.2 Review Specific to Porous Electrodes

The review so far has been concerned with scanning methods using planar electrodes. However, these planar electrodes did not give satisfactory performances. Therefore, there was the need to search for higher performance electrodes for the fuel cell. Consequently, considerable effort in research has been given to porous gas diffusion electrodes in recent times.

3.2.1 Theoretical considerations

In 1956, Ksenzhek and Stender [57,58] became the first to present theoretical treatments of galvanostatic charging transients of semi-infinite porous electrodes. They treated the case of combined double layer charging and

Faradaic reaction which was assumed to follow a linear polarization reaction. In a later development, Ksenzhek [59] considered galvanostatic transients for combined double layer charging and Faradaic reaction for electrodes of finite length. He took into consideration the influence of macro kinetic factors such as the transport of the material, and the passage of charge in the test and electrode areas. The author then plotted curves of overpotential with varying thickness of the porous electrodes as shown in figure 3.2. He used the slopes of the charging curves to determine the time of the double layer charging at any distance from the electrolyte end of the electrode. The author developed equations to determine the exchange current density and the specific capacitance of the electrodes. The treatment also included the effects of the external surface area of the electrode and of concentration polarization. He concluded that when the exchange current density was large, the electrochemical process could be regarded as virtually reversible and the polarisation characteristics of the electrodes could then be determined by a concentration phenomena.

Possey and Morozumi[60] followed up by presenting theoretical potentiostatic and galvanostatic charging transients of porous and tubular electrodes of finite length in the absence of Faradaic currents. They employed the one dimensional single pore model to derive the galvanostatic transient equations that are used to determine the exchange current density and the double layer capacitance of the electrodes. In addition, solutions were given for potentiostatic and galvanostatic single pulse measurements using square wave of current or voltage and for triangular currents or voltage sweeps. They also investigated the effects of external surface area and the conductivity of the metallic face on the exchange current density and the double layer capacity. All these presentations

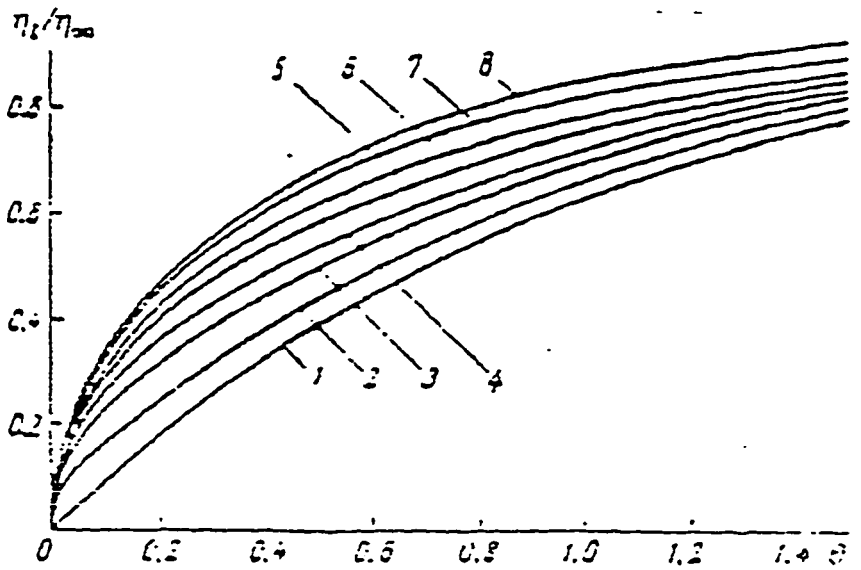

Figure 3.2: Charging curves for porous electrodes of various thicknesses. Reduced thickness δ:
1) 0; 2) 0.3; 3) 0.8; 4) 1.0; 5) 1.2;
6) 1.5; 7) 2.0; 8) ∞.

were theoretical. There were no experimetal work carried out to verify their conclusions.

Tiedman and Newmann[61] described a method for determining the double layer capacity. They explored the current response to a voltage step input function. Again, faradaic currents were neglected.

In 1969, Rangarajan[62] presented a comprehensive treatment of transient behaviour of porous electrodes under galvanostatic and sinusiodal pertubations. The concentration polarization and the ohmic activation were treated as generalised impedence. Response to other forms of input (eg.potentiostatic) could then be deduced under linear pertubation conditions. The author presented the model as an isotropic, homogeneous medium in the form of a transmission line. He derived equations for the determination of the double layer capacity and criticised earlier reports by Gunuvich and Bagotski[63] for using the linearised form of the current-potential relationships to find analytical solutions. He also derived equations for the cases of charging in the double layer regime, and activation ohmic polarisation. He used the methods of impedence. However, impedence methods are known to give only global values of the electrode parameters. In 1963, the same author[64] used a mathematical approach to show the importance of the use of linear relaxation methods. He explained that such mathematical treatment will reveal concealed phenomena such as a maximum or any distinct physical features. These output profiles could then be easily interpreted.

3.2.2 Experimental Considerations

Using unsteady state impedence methods, De levie[65] derived potentiostatic and galvanostatic charging transients for semi-infinite porous electrodes. Solutions for determining the double layer capacity were given. An equivalent model that is visualised as a 'transmission line' was used to derive the transient response to step functions in galvanostatic and potentiostatic modes. The author also represented both the planar and the porous electrode characteristics on an impedence plane. In addition, the depth of penetration and the influence of the curvature of the electrode surface on the values of the parameters were given. An exprimental verification of the equations were carried out using a radiometer GB11 impedence meter. The author used platinum brush electrodes and established that the double layer capacitance of porous electrodes behaved like a 'Warburg' impedence at a flat electrode surface. He then proceeded to present cases of diffusion and charge controlled phenomena. He found that the results of the exchange current density and the double layer capacitance to be in excellent agreement with that obtained from theory.

Austin and Gagnon[66] in part I of their communique presented theoretical treatments for determining the double layer capacity of porous electrodes. With the single pore model and making some practical assumptions, they presented equations to calculate the double layer capacitance and the exchange current density. The authors used triangular voltage sweeps in treating the transient response. In part II of their communique, the same authors used impedence triangular impulses to experimentally verify the equations developed in part I.

They worked with a NaOH solution and used Ni at 90 deg. C. The authors determined the double layer capacitance and the exchange current density and found them to be in good agrrement with literature values. They concluded that by using low sweep rates faradaic currents are negligible. However, faradaic currents may depend not only on the sweep rates but also on the concentrations of ions around the vicinity of the electrode.

3.2.3 Studies Pertaining to PTFE Bonded Electrodes.

Muud et al [67] studied the response of porous electrodes to various forms of impedence techniques. They used Raney nickel and silver catalysts for their studies of the alkaline fuel cell. In the case of the acid fuel cell, they employed a Tungsten Carbide (WC) catalyst for the hydrogen electrode. These were homogeneous electrodes. They then used a nonhomogeneous electrode made of glassy carbon for a comparative study. The authors discussed the influence of the various physical parameters of the electrodes on the frequencies of the applied instrument. By employing the raney nickel, the authors determined the charge transfer resistance and the double layer capacitances at low frequencies. They concluded that for the raney nickel electrode, the particle size was an important parameter that influenced the frequency of the impedence of the applied instrument and suggested that high efficiencies of the cell could be obtained by varying the particle sizes. They found that the inhomogeneous glassy carbon worked well as long as the process of activation was incorporated in the mathematical treatment of the results. The authors concluded that impedence methods are useful for characterizing the performance of porous electrodes but that such analysis should be based on models that take the

physical parameters into consideration.

Lu and France[68] studied the effects of of gas-phase transport on the performance of electrodes of fuel cells. They used special methods to enable them incorporate solid crystallized phosphoric acid in the PTFE electrode so as to block some of the hydrophilic pores. They then determined the voltage losses resulting from a predicted oxygen partial pressure drops in the electrodes. They loaded the cathode and anode electrodes with platinum of amounts 0.52 and 0.34mg/sq.cm respectively. They found that at any current density, the oxygen partial pressure drop decreased with increased air flow rate and that for a constant oxygen utilization, the film pressure drop increased with the operating current density. They calculated potential pressure drop at the highest current density (300mA/sq.cm) and the largest oxygen utilization (63%) was only 1.24%. Based on this, it was concluded that mass transfer resistance in the stagnant film was negligible. The authors also discussed the effects of pore diffusion in the backing layer, pore diffusion in the catalyst and the effects of air flow rates on the cathode performance. Finally, the authors found that the mearsured cathode potential losses at higher flowrates were in good agreement with predicted values.

Later, Hobbs et al [69] studied the application of pulse techniques to porous electrodes. They combined galvanostatic and potentiostatic modes to determine precise values of the intrinsic activity of the electrocatalyst, the support interactions and the effective electrochemical active area of the gas diffusion and gas evolution electrodes. The authors presented the theory of pulse technique and derived equations for determining the exchange current density, the double

layer capacity and the effective surface area of the electrodes. They used PTFE bonded electrodes and employed potentiostatic and galvanostatic transient techniques. They found that at times sufficiently near the double layer charging period, the effect of mass transfer was noticeable as the current density dropped, indicating that the double layer was sensitive to impurities and its value was higher than that of planar electrodes. They also found that the performance of the Pt black electrode was reduced to about 40%-50% due to large bubbles that were formed and got attached to the external surface of the electrode. They therefore concluded that in addition to mass transfer and ohmic effects, the performance of hydrogen electrodes is affected by

1. the reduction in the electrochemically active surface layer due to gas bubbling formation in the internal pores. They expelled the electrolyte.
2. the large gas bubbles sticking to the outer surface of the electrode restricting diffusion of electrolyte.

Katan and Carlen [70] studied the pertubations of concentration gradients in porous zinc electrodes. They used ten commercial zinc electrodes to simulate conditions of the reaction profile that takes place in the pores of the porous electrode structure. The electrolyte used was KOH solution. The authors estimated the OH^- concentration profiles in the pores by utilizing open circuit potentials. They concluded that the derived concentration profiles indicated an increase of $(OH)^-$ with concentrations varying from 7.7M to 8.4M at the pore mouth where ZnO was precipitated and the OH^- released. This increase of OH^- concentration will increase the amounts of current and hence improve the

performance of the electrodes.

Most of the investigations that have been reported so far used impedence measurements to determine the parameters of interests. However, impedence measurements are known to give only overall performances and it is therefore doubtful that such results are reliable as a criteria for use to determine the performances of porous electrodes. In addition, analytical solutions that employ impedence are very cumbersome to handle mathematically since they use real and imaginary quantities.

In order to get rid of using impedence, Rangarajan[71] in 1973 introduced the concept of exponentially decay current technique to study the response of porous electrodes using direct current. This form of relaxation was concerned with the interplay of activation, linear diffusion, and chemical reaction in the bulk electrolyte. The author discussed the relevance of the exponential decay current technique by using a parametric approach. He also discussed cases of single pulse and decreasing current techniques. Finally, Rangarajan et al [72], again examined theoretically and experimentally, the two parameter current controlled input functions (current ramp and exponentially decaying current) for the determination of the double layer capacitance of porous electrodes. The author employed the flooded pore model to derive equations for the galvanostatic and potentiostatic exponential decay methods. To enable him experimentally verify his equations, he used a Ni plaque electrode and a 4M NaOH solution at 25%. He also used a teflon-bonded platinum on Pt screen as another electrode with the same concentrations of electrolyte in the second part of his experiments. He obtained a double layer capacitance of 454mF and an

exchange current density of $1x10^{-6}A/cm^2$ which agreed very well with literature values for the case of the teflon bonded electrode.

From the previous investigations, it is observed that most of the work employed impedence methods. However, it is known that these impedence techniques do not give precise values. In addition, the porous electrodes used all have different methods of preparation. It is therefore important to adopt a method that will use direct current and be free from the scanning problems that were earlier pointed out in this review. The exponential decay current technique uses direct current. Apart from this, the exponential decay current has certain unique properties (details are given later) that make it adequate for the experimental work that will be carried out in this research.

CHAPTER 4

4.0 EXPERIMENTAL

4.1 Experimental Apparatus.

The apparatus used in the set-up for studying the exponential technique is shown in figure 4.1. The following make up the components of the set up.

4.1.1 Half Cell

The half cell consists of two chambers each of which is made of plexi glass. One chamber is used to admit the gas into the half cell unit and the other chamber is used to hold the electrode between the gas and the electrolyte. Protruding from the electrode chambers are two nickel wires that serve as current collectors from the electrodes. A white polyteflon fluoro ethane (PTFE) ring acts as a seal against any mixing of the electrolyte and gas. The other accessories include a cylindrical container (about 2litres in volume) with its lid and bolts to screw the two half cells together.

4.1.2 Potentioscan

The potentioscan is a Winking POS 73 type. It is capable of being used for both galvanostatic and potentiostatic control studies. It also has an additional facility for generating rectangular, triangular and sinusoidal impulses.

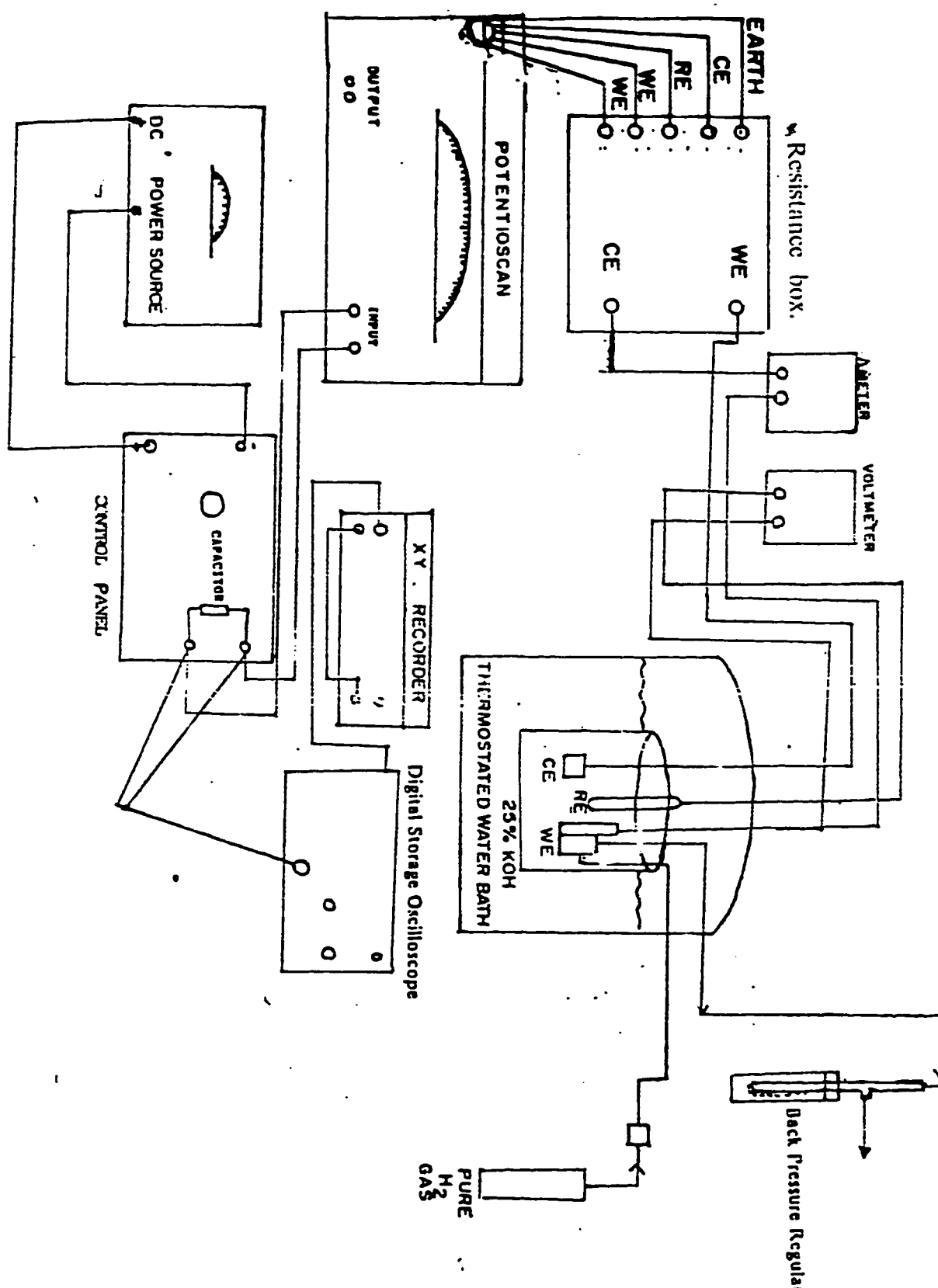

Figure 4.1: Experimental Set-up for the Exponential Decay Current Method

4.1.3 Digital Oscillioscope

The digital oscillioscope is of type PM3302,001. it can be used to capture events of the order of microseconds. In addition, it has two inlets A and B which can be used for simultaneous monitoring of two independent events.

4.1.4 Recorders

The XY recorder is of type PM 8133 and it is used to record the exponential display from the oscillioscope. The other type is the XT recorder. This is of type PM 8252A. It is used to record the triangular wave response.

4.1.5 Digital Thermometers

The model 2751-K digitron instrument was used for measuring the temperature. This instrument which is digital was precalibrated and tested with a standard mercury- in- glass thermometer.

4.1.6 Flowmeter

Brooks thermal mass flowmeter was used to measure the flowrate of the H_2 gas. The instrument has four different channels available for four different measurements.

4.1.7 Gas-Feed System

The H_2 gas is contained in a hydrogen cylinder fitted with a Matheson - made pressure guage. Plastic and rubber tubings are used to send the gas to the half cell containing the KOH solution.

4.1.8 Electrodes

Raney Ni / PTFE sheets were provided by DLR of Germany and was used as the hydrogen electrode. The counter electrode was made of a Ni foil and was also supplied. The reference electrode was a Hg / HgO one.

4.1.9 Auxillary Equipment

One of the auxillary devices is the offset device. This was deviced in our laboratory to offset part of the overvoltage so that the recorder could get the plots within the dimensions of the graph paper.

Another auxillary device is the panel. The panel contained the capacitances and the resistors in series. This procedure enabled the desired time constant to be easily set up. Other auxillary equipment included a stirring rod and a weighing machine.

4.2 Materials.

The potassium hydroxide that was used for the studies was obtained from Aldrich Chemical Co. and had a minimun assay of 85%.

The distilled water was obtained from the laboratory distilled water reservoir.

4.3 Experimental Procedures

The experimental set-up for both the exponential decaying current and the triangular wave are identical. Figure 4.1 shows the set-up for the exponential decaying current technique.

4.3.1 Preparation of KOH solution

A 25% KOH solution was prepared for the studies. First, the empty cylidrical plastic container was weighed and recorded using an electronic weighing machine. Next, a predetermined amount of KOH pellets were added to the container and the weight again recorded. The difference between the two weights gave the amount of the pellets (423g) used. After weighing, distilled water of 1500cc was added to dissolve the pellets. A plastic rod was used to stir the solution. The solution was then left to cool as the dissolution generated a lot of heat.

4.3.2 Assembling Half Cell Unit

First of all, a circular piece of the hydrogen electrode 2.5cm in diameter was carefully cut with a scissors and inserted into one of the holes of the chambers that make up the half cell. The plastic flappy seal was then used to seal the top of the hole. Using the screws, the two chambers were screwed together. Next, the unit was screwed to the cover of the plastic container. The inlet to the container was connected to the hydrogen gas via the plastic tubes. The exit was also connected to the cylindrical glass tube containing the water. The water column served to regulate the back pressure which develops in the gas chamber. The adjustable long rod was varied in height to obtain the required gas pressure.

The hydrogen cylinder was opened and the half cell unit was dipped into the KOH solution in the plastic container. The plastic container and the half cell unit were then placed in a thermostatic bath equipped with a stirrer. The Brooks flow control read out was used and the desired flowrate obtained by turning the control channel.

Following this assembly, the reference electrode and the counter electrodes were inserted into the KOH solution through the two small holes provided on the plastic lid.

4.3.3 Electrical connections

After assemblying the half cell unit, the potentioscan was connected to it through a variable resistance box. The potentioscan was used to send the

current in a galvanostatic mode to cell. The potentioscan was again connected through the input control to the panel on which are the capacitor connections. The panel was connected to the digital storage oscillioscope which was inturn connected to the XY recorder. The high impedence multimeter (ammeter) was connected to the working electrode and the resistance box to measure the current from the potentioscan. The voltmeter was connected to the reference electrode and the working electrode to measure the potential drop across the cell.

4.3.4 Activation of Electrodes

In order to ensure that the electrodes were working as expected and will give reproducible results, the system was put in activation mode. For the activation, the potentioscan was turned on and the selector knob turned to the "I" position. A constant current of 25mA was passed to the cell by using the initial voltage selector knob. Both the temperature and the open circuit voltage (OCV) were taken. The system was left in this position for a day. Runs were carried out to determine whether the activation was complete. First the selector knob was turned off and the OCV recorded. Secondly, current was drawn from the cell at intervals of 12mA and the corresponding potentials were recorded. At the end, the current is decreased in the reverse direction and the potentials are again recorded.

4.3.5 Exponential Decay Method

The following steps were carried out in order to generate the exponential

decay current.

1. The knob on the panel was depressed and the capacitor charged in the process.
2. The digital oscillioscope was turned on and by adjusting both the time/division and the amplitude/division knobs, the event was captured and displayed on the oscillioscope.
3. The XY recorder was used to record the profile from the oscillioscope display.
4. In order to generate another profile, the knob is depressed once more to discharge the capacitor.
5. The knob is then depressed a second time for the display.
6. Finally, a second capacitor of different capacitance was used to replace the first and the procedure carried out in the same manner.

The response from the half cell is displayed by using a procedure similar to the one just described. In this case, the panel was now connected to the reference and working electrodes of the cell. Then the knob was depressed and the display captured.

Next, the temperature of the bath was raised to a desired value and the process repeated all over starting from the generation of the current to the response of the cell. Three more different temperatures were done.

4.3.6 Triangular Wave Method

The diagram for the triangular wave method is shown in figure 4.2. This time the offset device was used so that the response plots were conveniently obtained on the graphs of the XT recorder. The XT recorder and the offset device were electrically connected. The potentioscan and the half cell were also connected as usual through the variable resistance box. The current side of the potentioscan was then connected to the XT recorder.

In order to carry out a run, the following procedures were taken.

1. The potentioscan was turned on and put in a galvanostatic mode as described earlier.
2. The desired scan range was obtained by using the scan knob on the potentioscan. In this case, the attenuation knob was set to 1000 and the scan rate was then turned to the desired value.
3. Both buttoms of the triangular and periodic functions of the potentioscan were depressed.
4. The pens of the XT recorder were brought down and the chart speed selected. The resulting plots obtained were taken and analysed.

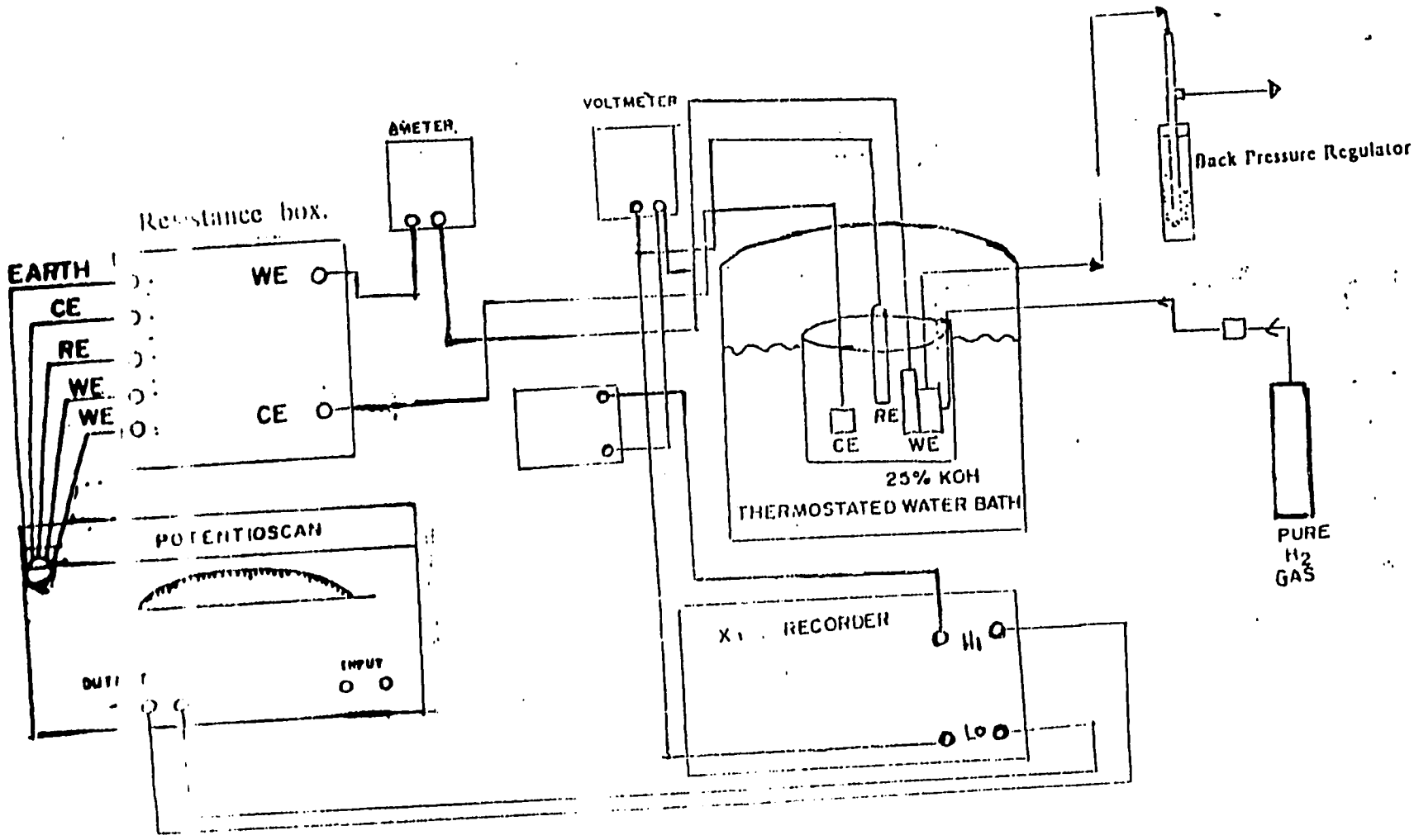

Figure 4.2: Experimental Set-up for the Triangular Wave Current Method

CHAPTER 5

5.0 Results and Discussion

The relevant parameters that characterize the performance of the porous gas diffusion electrode have been determined. The results and discussion will be reported in the following order:

Experimental Data: This section will summarize the data obtained by using the exponential decay current and the triangular wave of current techniques.

Activation: Activation is important for the fact that it ensures that results are reproducible. This section compares the two plots obtained when carrying out activation. One of the plots was obtained by drawing current from the cell in an increasing manner (forward) whereas the other curve was obtained in the reverse direction of decreasing the current drawn (backward). The comparison showed excellent reproducibility.

Determination of Exchange Current Density: This section discusses the determination of the exchange current density for both the exponential and triangular wave current techniques. First, the section discusses the nature of the curves obtained for the input and response funtions of the exponential decay current. Secondly, the section covers the straight line plots that are obtained from the

response curves. Next, a discussion of the straight lines combined under one single plot is presented. The value obtained for the exchange current density is compared with values obtained by using other porous electrodes and planar electrodes as reported in the literature. Finally, the section concludes with a comparison of of the values of the exchange current densities that are obtained under the same experimental conditions.

Determination of the Double Layer Capacitance: The results of the calculations of the double layer capacity are presented. The value of the double layer capacity is compared with with the value reported in literature. The reason for the high values (obtained by using the triangular wave of current) compared to the exponential decay current technique is given.

Determination of Activation Energy: determination of the energy of activation is presented in this section. First of all, the procedure used to obtain the plot that leads to the analysis is given. A comparison of the value of the energy of activation is made with values obtained from literature. An explanation is given for the small value of the activation energy obtained.

Determination of the Surface Roughness Factor: The importance of the surface roughness factor (RF) is discussed. The equations used to calculate the RF values are presented.

Faradaic Currents: The values of the exchange current densities are used to asses the importance of including Faradaic currents in the two techniques used in this study.

(All figures and tables with titles 'A' refer to appendix A)

5.1 Experimental Data

Exponential Decay Current Method

The experimental data that were obtained for the exponential decay current are reported in table 5.1.

A sample of the input and the response diagrams of the exponential decay current method is shown in figures 5.1A and 5.2B. As shown in figure 5.1A, the input Δi is measured by counting the number of divisions in the input profile and using the corresponding scale to obtain the value.

For example, (Figure 5.1A)

Total no. of divisions (Δi) = 4.5

Corresponding scale = 20mV/Div.

A one ohm resistor was connected in series to convert the readings in this case directly to mA. Therefore,

Δi = 4.5 x 20mA = 90mA

TABLE 5.1: Data for the Input and Response of the Exponential Decay Current

TEMP.(Deg.C) (Deg.C)	INPUT		OUTPUT	
	Cap_e (μf)	Δi (mA)	η_{max} (mV)	$t_{max} \times 10^{-6}$ (S)
30	0.01	36	2.0	15.0
	0.047	68	20.0	20.
	0.22	85	100	24.1
	0.47	90	205	28.5
	1.0	91	285	30
	2.2	95	300	33.5
42	0.01	36	2.0	10.0
	0.047	70	17.4	21.
	0.22	90	100	32.4
	0.47	95	215	38.1
	1.0	95	440	47
	2.2	100	560	59.0
48	0.01	38	2.0	13.0
	0.047	70	15.0	25.
	0.22	95	85.0	34.0
	0.47	95	195	35.1
	1.0	94	380	49.5
	2.2	99	665	59.3
65	0.01	40	2.0	13.0
	0.047	70	16.0	22.
	0.22	90	190.0	33.2
	0.47	100	190.	30.4
	1.0	94	380	53.0
	2.2	115	255	60.6

$$\ln\frac{\eta_{max}}{\tau\Delta i} = \ln(1/C_T) - \frac{\alpha}{\beta}t_m$$

Exponential Decay Current Method

Temperature : 30°C

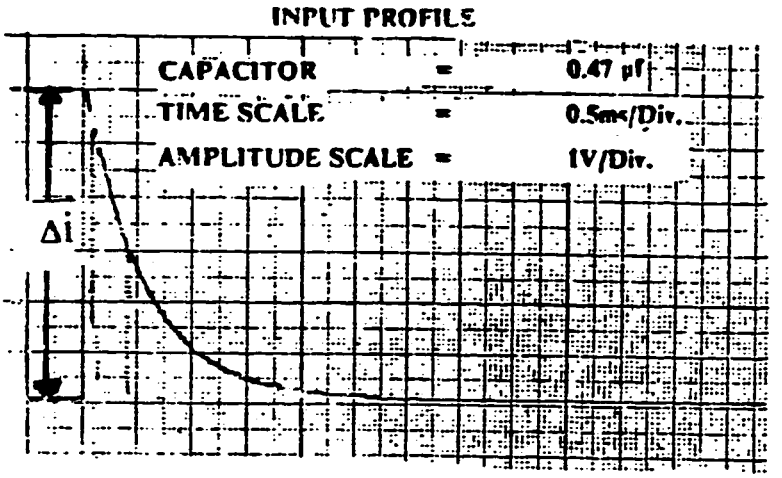

A

Figure 5.1 Sample Input Curve for the Exponential Decay Current Method.

Exponential Decay Current

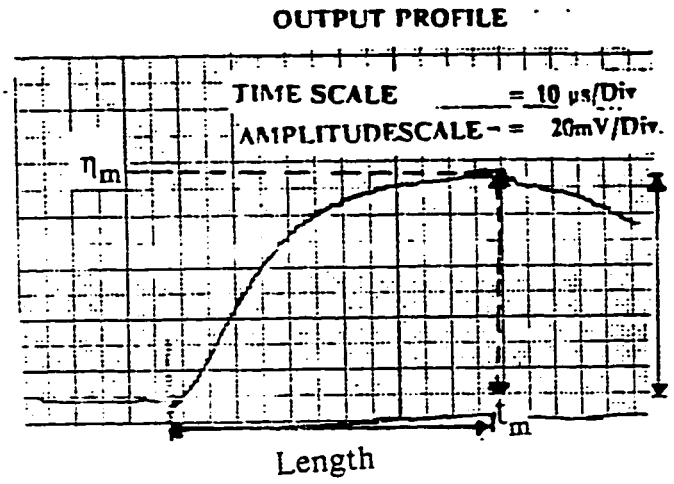

B

Figure 5.1: Sample Response of the Exponential Decay Current

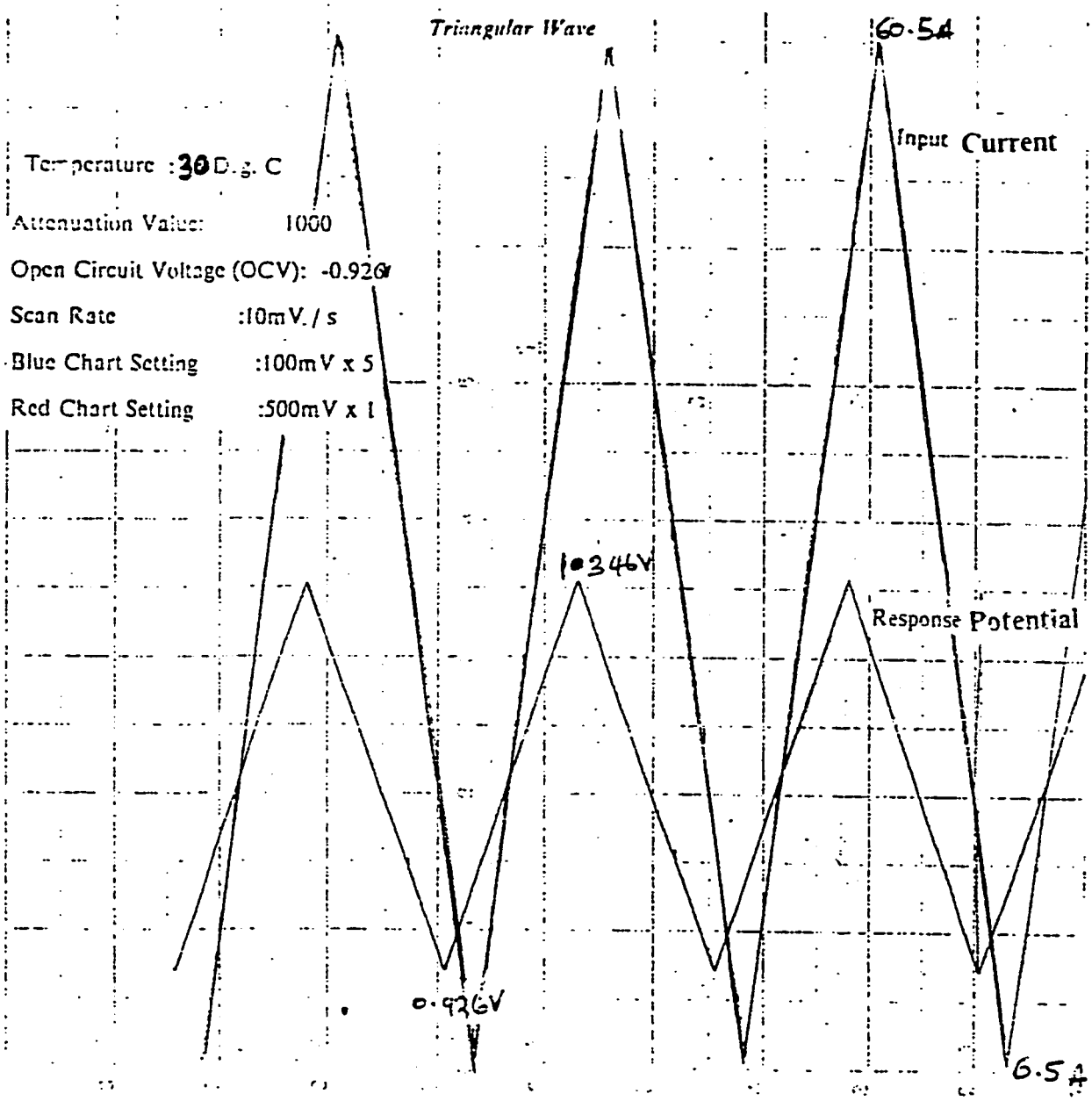

Figure 5.2: Sample Input and Response Curves for the Triangular Wave Current Method.

Potential Change = 1.346 - 0.926 V

Current (P/2) = 60.5 - 6.5 mA

= 54mA

(Note :The current at (P/2) is not a current change. An offset device was used to enable the plot to come on the graph. This value was not initially zero).

The values for the rest of the temperatures were obtained in a similar manner and are shown in table 5.2.

5.2 Activation

This is the pretreatment of the hydrogen electrode. The results obtained from the activation runs for both forward and backward runs are shown in Table A.1. From the two runs, a comparison of the activation at the same temperature indicates a maximum deviation of 5.9 percent. This reflects a measure of good reproducibility.

5.3 Method of the exponential decay current

5.3.1 Determination of the exchange current density

A sample of the input and response curves obtained during the exponential decay current method was shown in figure 5.1 A and B, respectively. A

TABLE 5.2: Data for the Input and Response of the Triangular Wave of Current Method

TEMP. (Deg.C)	INPUT Scan Rate (mV/s)	OUTPUT Period (s)	OUTPUT Current (T/2)mA	OUTPUT Potential Change(mV)
30	10	180	54	420
42	20	177	65	220
48	20	110	83	100
65	20	120	100	98

capacitor of 0.4 microfarads was used to generate the input curve. As expected, it is observed that the input current decays exponentially. When current is passed through a capacitor it becomes charged in the process. During discharge, capacitors give decaying exponential currents. This is the phenomenom observed in figure 5.1A. In figure 5.1B a maximum is observed. The physical explanation for this maximum is as follows. Initially, the voltage of the cell increases because of the sudden addition of the input pulse current. The increase is soon halted due to the decaying nature of the applied current. The exponential form of the decaying current then drives the voltage of the cell even lower and hence there is observed a turning point on the response curve. This point is the maximum.

As expected from the predictions of the theory, plots of $\ln\frac{\eta_m}{\Delta i\,\tau}$ versus t_{max} were made for the results of the exponential decaying current technique and a series of straight line fits were obtained by using linear regression on IBM computer graphics. Tables A.2 to A.5 give the values of the readings from the oscillioscope when the electrode is perturbed with the input current pulse. Values of the response voltage with time are also tabulated on tables A.6 to A .9.

In order to plot for the straight lines, tables A.1 to A.15 were constructed. Alternatively, the values were fed straight into the IBM computer. The resulting figures are shown in Figures A.1, A.2, A.3, and A.4. for the temperatures 30, 42, 48 and 65 deg. C. respectively. A combined plot of the four straight lines is shown in figure 5.3. Within the limits of experimental error, the slopes and the intercepts of the straight lines were used to determine both the exchange current densities and the double layer capacities.

The values obtained for the exchange current densities in the given ranges of temperature are reasonable. Rangarajan et al{72} reported an exchange current density of $1 \times 10^{-6} \frac{A}{cm^2}$. They worked with a NaOH solution and at a temperature of 80°C. At the maximum temperature of 65°C. the results show an exchange current density of $11 \times 10^{-6} \frac{A}{cm^2}$. This value is reasonable compared to the reported value. The electrodes used in these experiments have been designed to have characteristics that are different from what is reported in the literature as a result, the higher value obtained only goes to emphasise the fact that the electrodes used in the experiments have higher performances. As a matter of fact, this is what is expected from the improved design of the electrodes.

$$\ln\frac{n_{max}}{\tau\Delta i} = \ln(i_o/C_T) - \frac{\alpha}{\beta} t_m$$

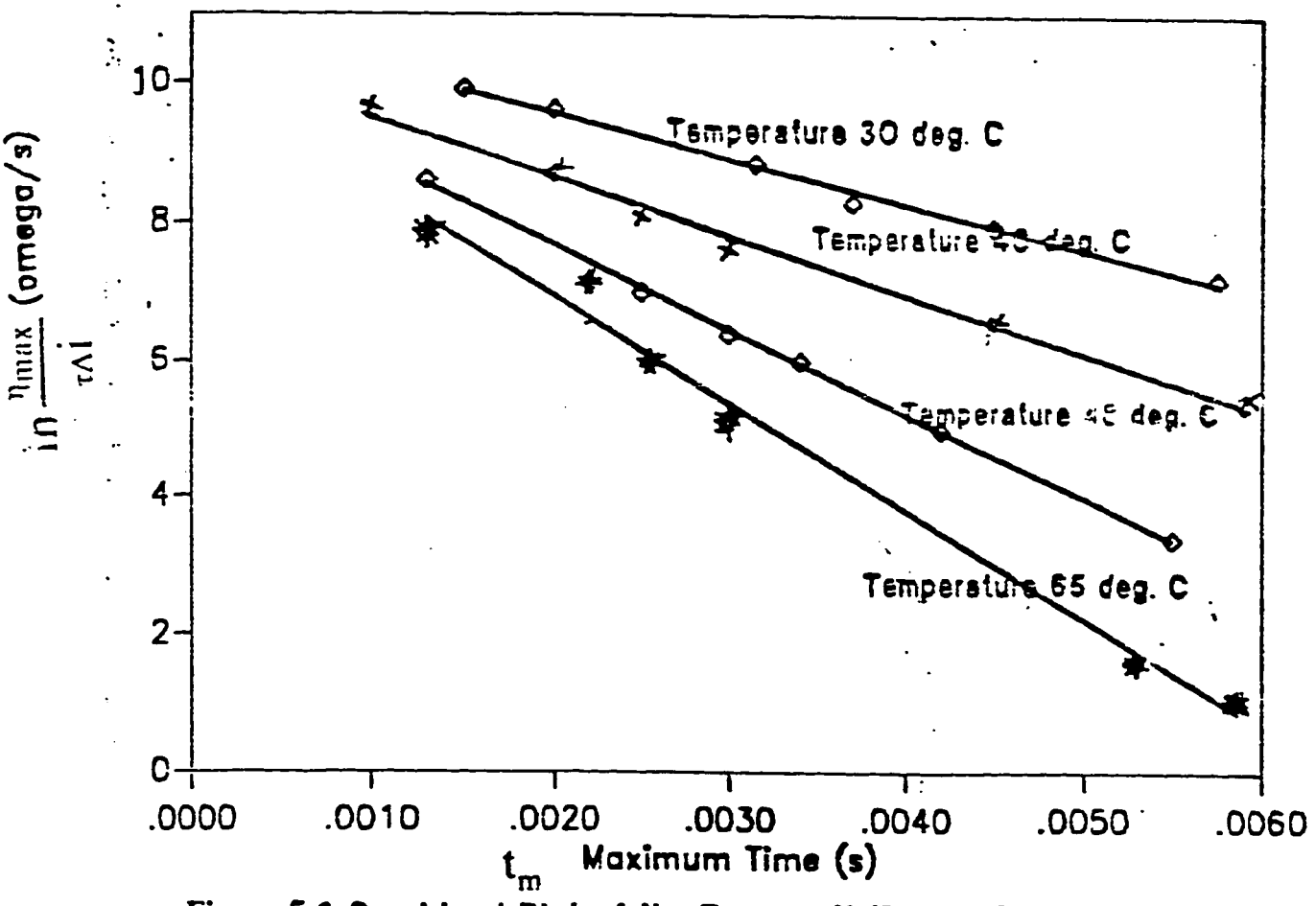

Figure 5.3: Combined Plot of the ExponentialDecay Current Technique.

These values obtained for the exchange current densities were also compared with values obtained by Celiker[73]. The values of Celiker were in the range of $(0.76 - 4.5)x10^{-6}A/cm^2$ for a temperature range of 25-75 deg. C. Celiker worked with the same electrode and electrolyte concentration as used in this investigation. However, he used steady state technique and a model (he developed) to obtain the exchange current densities. The values obtained in this study agree with those values of Celiker. Apparently, the difference is due to the fact that steady state measurements give overall values whereas unsteady state measurements give precise values. In fact, the unsteady state values serve as a check for the values obtained by using steady state methods.

This value was again compared with that of planar electrodes. Tibor also working with a Ni planar electrode in a 2.0N Na_2SO_4 solution obtained an exchange current density of $2 \times 10^{-9} \frac{A}{cm^2}$. Thus, it is clear that the porous electrode structure gave a higher exchange current density and hence a better performance.

Figure 5.4 shows a plot of the exchange current density against temperature. From the plot, it is found that the exchange current density increases with temperature. In addition, it is realised that the current density is a strong function of the temperature since for a change of 10 deg. C of temperature the exchange current density doubled its value. This behaviour culminates from figure 5.3 where the straight line plots were observed to have steep gradients with increasing temperature. The results are not surprising because the gradients in the straight line plots represent a ratio of the kinetic to

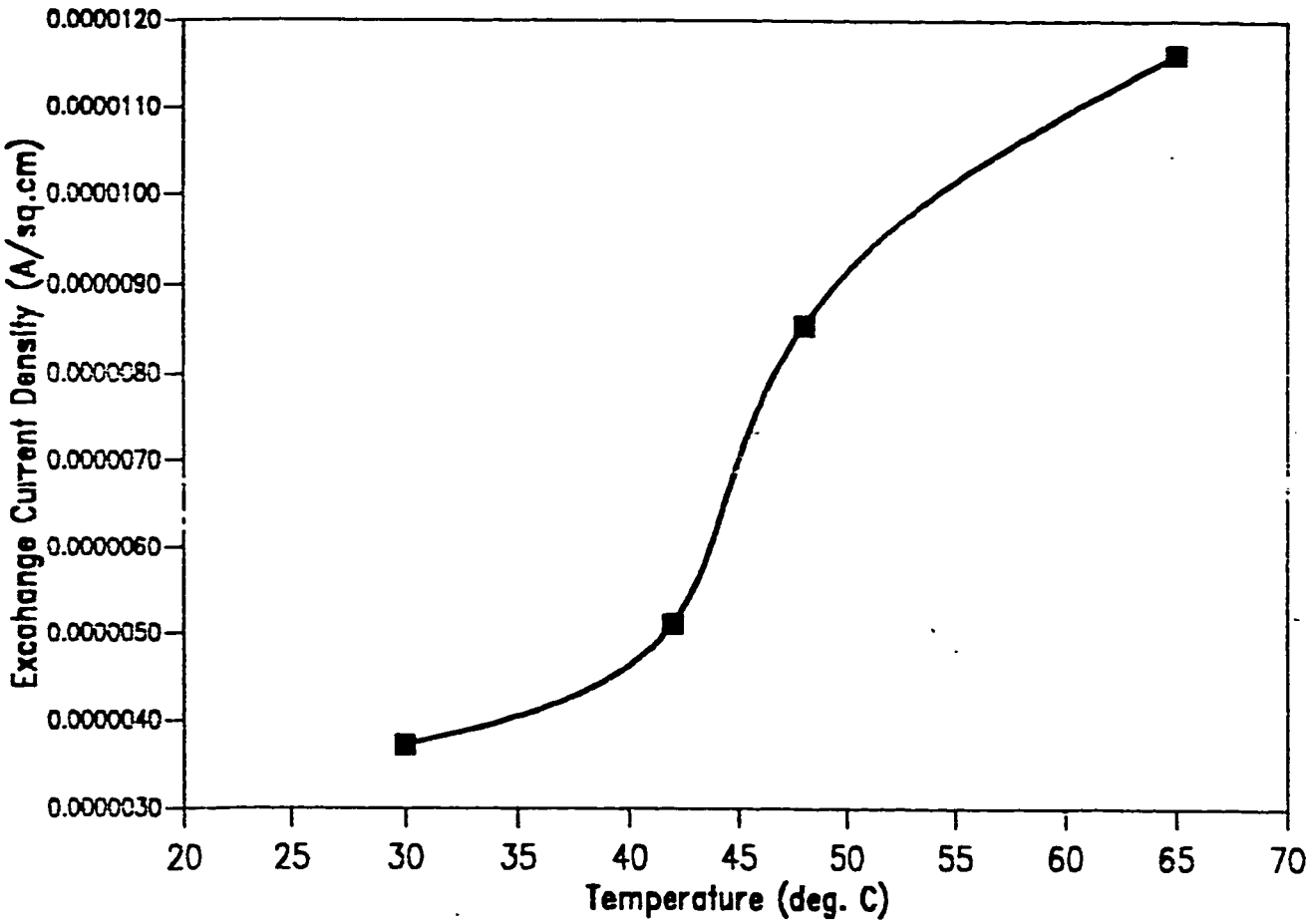

Figure 5.4: Plot of Exchange Density VS. Temperature.

the mass transfer phenomena. As the temperature increases, the kinetic behaviour predominates and so the gradients will have to increase since the mass transfer invariably remains constant.

5.3.2 Determination of the Double Layer Capacitance.

The calculations for the double layer capacity using the exponential decay current method is illustrated in appendix B. The range of the values obtained in this study is (91-104)mF for the temperature range of (30-65)deg.C. Again Rangarajan reported a value of 435mF while working with the same electrolyte and electrode as mentioned earlier. The values of the double layer capacitance did not increase significantly with temperature as compared to the trend observed earlier for the exchange current density and temperature. The reason for the low trend exhibited by the double layer capacity is that since the double layer is more dependent on the concentration, the increase in temperature did not have much effect on the amount of charge accumulated in the layer. The concentration gradient arising from the increase in temperature might be responsible for the small increase of the capacitance.

5.4 Method of the Triangular Wave of Current

The purpose of carrying out the triangular wave current method is to get values of some of the parameters that will serve as basis for comparison with the exponential decay method since both experiments were carried out under the same conditions. The input current and the response voltage were simultaneously recorded and a sample of this was already shown in figure 5.2.

The data for the triangular wave technique is shown in table 5.3. The calculations for the exchange current density are illustrated in Appendix B. The results from the calculations are shown on table 5.4.

5.4.1 The Temperature Dependence of the Exchange Current Density.

A comparative results of the two techniques are shown on table 5.5. First of all, it is observed that the values of the exchange current densities obtained using the triangular wave method were in excellent agreement with the exponential case. Secondly, the exchange current densities increased with increase in temperature. A similar trend of a plot of the exchange current density with the temperature is expected as shown already in figure 5.4. The lower portion of this graph could be linear but as the temperature increases the shape takes an exponential form to level at the top. The explanation is given as follows: Initially, only a small number of particles are charged. As the temperature increases, there is a corresponding increase in the number of particles being charged. This situation will result in an enormous currrent being produced and the overall effect is an increase in the exchange current density. However, as more charged particles are used up, there is depletion at the surface of the electrodes. The effect of the depletion leads to the creation of a concentration gradient. In addition, the effects of diffusion are also expected to set in although these might be minor. As a result, there is a drop in the charge being passed through the system and the current does not increase any further.

5.4.2 Determination of the Double Layer Capacitance

The calculations for the double layer capacitance of the triangular wave of

TABLE 5.3: Response Values for the Triangular Wave Technique

SETTINGS:

Attenuation Value: 1000

Open Circuit Voltage (OCV): -0.926

Scan Rate :10mV / s

Blue Chart Setting :100mV x 5

Red Chart Setting :500mV x 1

T is the Period

Readings Obtained from Plots

Temp. (°C)	Period (s)	Potential Change (mV)	Current(T/2) (Amps) * 10^3
30	180	420	54
42	177	150	65
48	110	350	83
65	120	100	100

TABLE 5.4: Results for the Triangular Wave Technique

EXCDENSITY :Exchange Current Density

DOBLACAPACITY:Double Layer Capacity

Temperature (°C)	EXCDENSITY $(A/cm^2)*10^6$ -	DOBLACAPACITY (mf)
30	3.72	167
42	5.11	207
48	8.54	223
65	11.60	294

current technique is illustrated in appendix B. The results are tabulated on table 5.5. It can be inferred from this table that the double layer capacities obtained by using the exponential decay current technique increased with temperature. However, the values did not increase significantly with temperature compared to that of the trend of the exchange current density that was earlier discussed.

The values of the double layer capacities obtained by using the triangular wave method were substantially higher than the corresponding values obtained by using the exponential decay current method. Table 5.5 shows the comparative results. The difference in the values can be accounted for by the fact that in the triangular wave technique, the experiments were carried out at slow times. In the exponential decay current method the times are very fast-microseconds. The double layer is a combination of a Hemholtz layer and a diffuse layer. The diffuse layer depends to a large extent on the concentration of the electrolyte. Therefore, as enough times elapes in the triangular method, the diffuse component of the double layer increases due to the changes in the concentration of particles near the metal surface and the solution. This implies the double layer capacitance is extended, as more charge is needed in the direction of the electrolyte. The values obtained by using the exponential current decay method is more reliable than those values that were obtained by using the trianguar decay method. The reason for this conclusion is that during the triangular sweep there is a change in the potential. This change will affect the double layer capacitance. However, the exponential decay current method does not suffer from this phenomenom of change in potential.

TABLE 5.5: Comparative Results of the Exponential and Triangular Currents

EXCDENSITY :Exchange Current Density

DOBLACAPACITY:Double Layer Capacity

Temp.	EXCDENSITY (A/cm^3)*10^6			DOBLACAPACITY (mf)	
(°C)	Expon.	Tri.	Deviation	Expon.	Tri
30	4.0	4.05	7	91	167
42	6.42	5.11	20	93	207
48	9.28	8.54	7.9	98	223
65	11.9	11.6	2.5	104	294

5.5 Determination of Activation Energy

The values of the exchange current densities obtained by the exponential decay current technique were used to construct table 5.6. A plot of the logarithm of the exchange current density versus the inverse of the temperature is shown figure 5.5. The slope of the straight line resulting from the plot was used to determine the activation energy. The value found for the energy of activation is 4.15 Kcal / gmol. Again there is no reported literature for the value of the energy of activation for this electrode however, in the literature this value seldom exceeds 10Kcal/gm mol(30). The value obtained is within the expected range. The small magnitude of the value also shows that by using porous electrodes and with the special preparation techniques, the activation energy can be reduced. It is to be noted that an alternative way of reducing the activation energy will be to increase the potential. An increase in the potential in this circumstances is obviously at the expense of the fuel cell, hence the advantage of using the improved perfoming electrodes.

5.6 Determination of the Surface Roughness Factor

The surface area of porous electrodes that is effective for participation in electrochemical reactions is reliably estimated from the double layer capacity. A direct measure of the effective surface area will be to determine the surface roughness factor. The values of the double layer capacitance (C_T) are used to determine the surface roughness factor. These values are the total capacitance given by

TABLE 5.4: Data for the Determination

of the Activation Energy

T ($^{\circ}K$)	$1/T * 10^3$ - ($/^{\circ}K$)	EXCDENSITY (i_o) (A/cm^2)*10^3	ln(io)
303	3.3	3.86	-12.46
315	3.17	6.42	-11.96
321	3.12	9.28	-11.59
338	2.96	11.9	-11.34

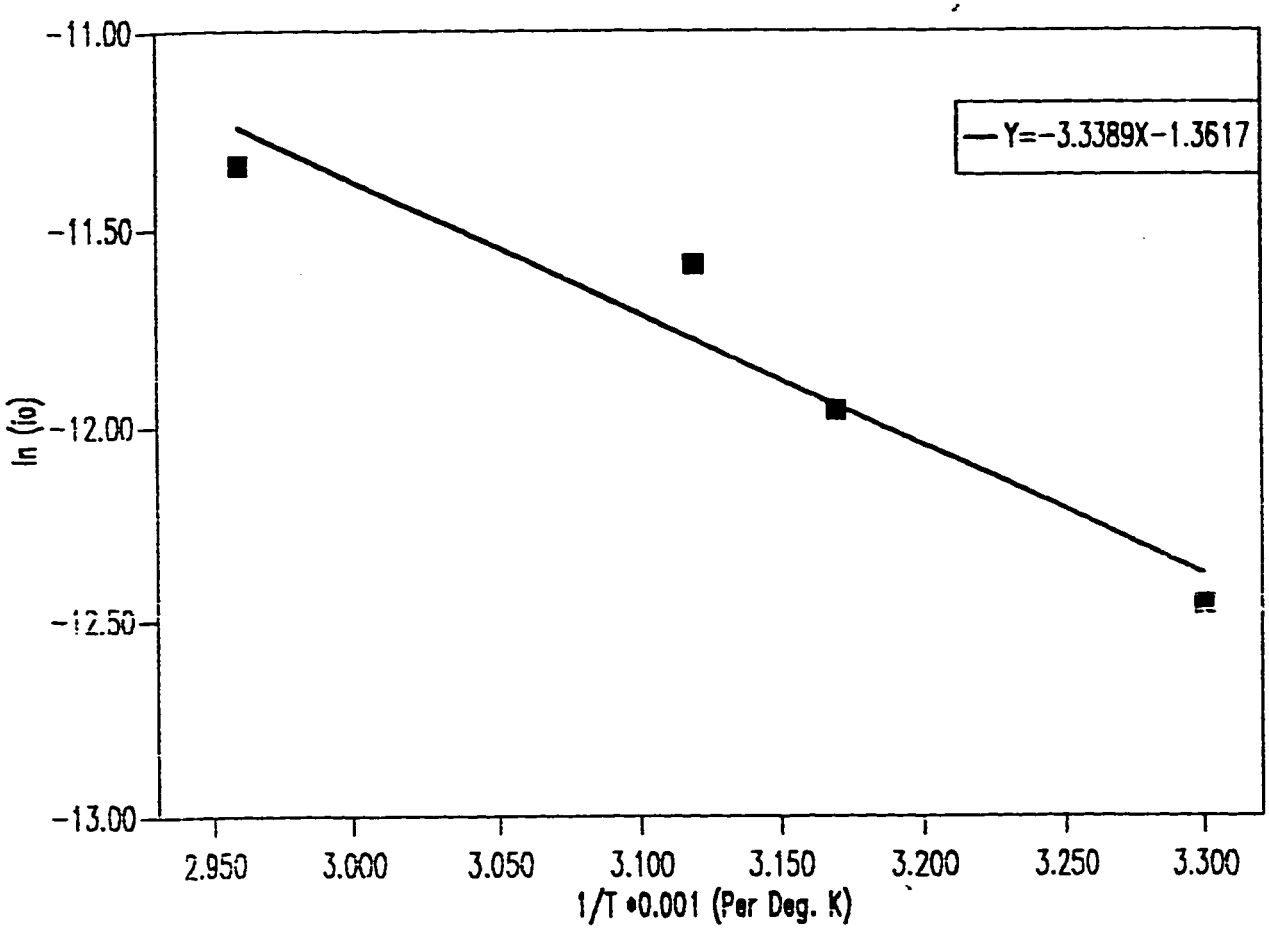

Figure 5.5: Plot of Exchange Current Density Versus Inverse Temperature

$$C_1 = S\,C\,I. \tag{57}$$

The surface roughness factor is obtained from the equation

$$RF = \frac{C}{C_{ideal}} \tag{58}$$

where C_{ideal} is the capacitance of the smooth electrode surface. The value is given by Ksenzhek as $17\mu/cm^2$

Table 5.7 shows the values obtained for the temperature range of interest. A plot of the surface roughness factor and temperature is shown in figure 5.6. There is a definite increase in the RF values with increase in temperature. Thus, as the temperature increases, more of the active nickel component are exposed for the reactions to take place. Hence an increase in temperature favours the production of currents.

5.6 Faradaic Currents

Faradaic currents are associated with charge that crosses the electode boundary by electron transfer. Depending on whether it is the charge transfer step that dominates or other processses such as diffusion and polarisation, the magnitude of the faradaic currents could significantly affect the parameters investigated in this study. In the exponential current decay technique, the faradaic currents are incorporated in the derivation of the equations to be used in calculating the exchange current density and the double layer capacitance. On the other hand, the triangular wave method does not take faradaic currents into consideration. However, the experimental results for both the exponential and

TABLE 5.7 Results of Surface Roughness Factor

RF : Surface Roughness Factor

Temp.(Deg. C)	RF($(cm^2)/cm^2)*10^4$
30	36
42	45
48	49
65	64

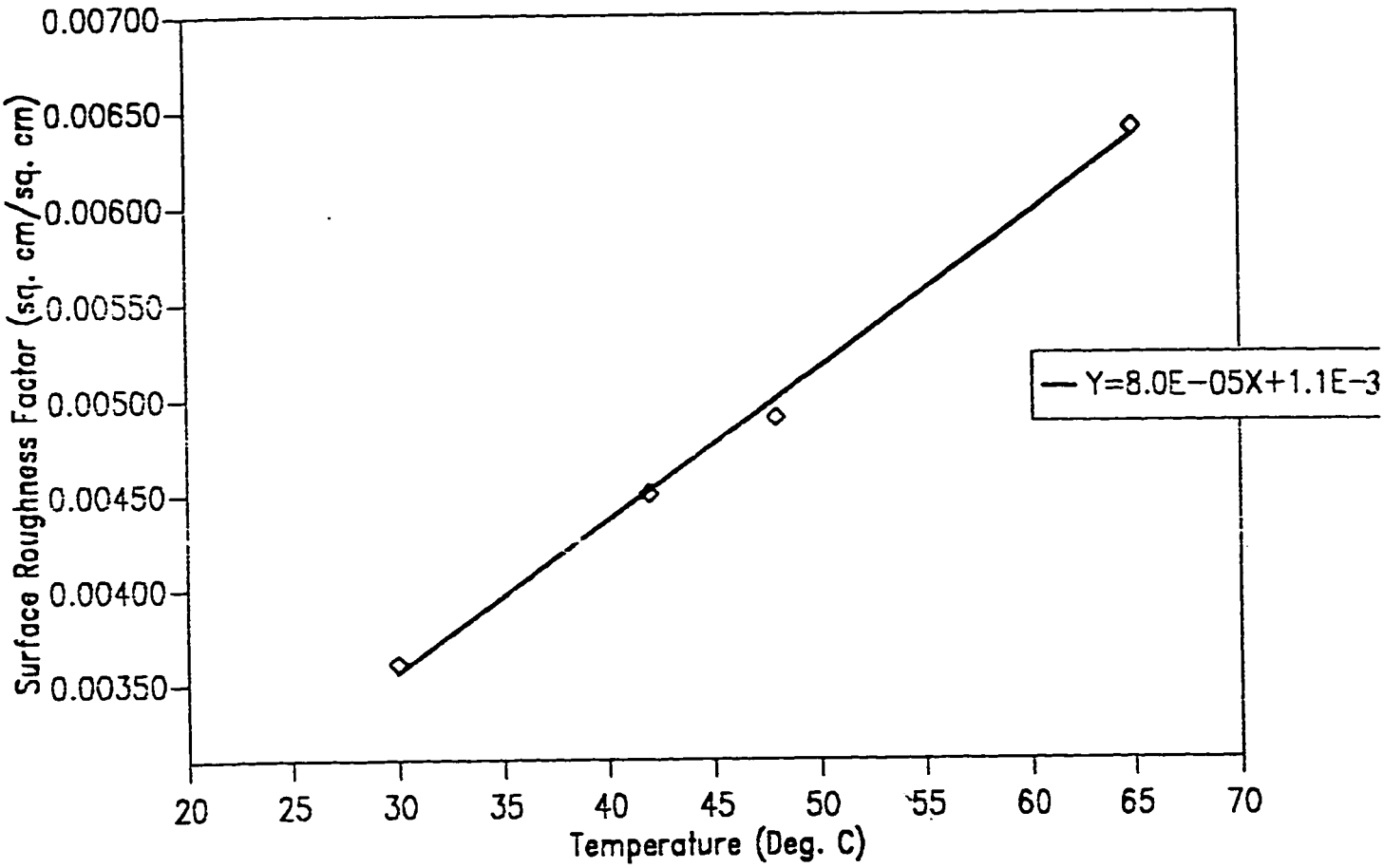

Figure 5.7: Plot of Surface Roughness Factor and Temperature.

triangular methods do not differ significantly. The maximum difference was 6 per cent. Intuitively, it can be concluded that the contribution of faradaic currents to the overall determination of the parameters of interest is negligible therefore supporting earlier techniques that neglected faradaic currents.

CHAPTER 6:CONCLUSIONS AND RECOMMENDATIONS

6.1 Conclusions

In this thesis work, the important parameters that characterise the performance of the alkaline fuel cell electrodes have been determined using both the exponential decay current and the triangular wave techniques. From the study, the following conclusions have been reached.

1. The values for the exchange current densities determined from both the exponential decay current and the triangular wave were found to be in good agreement and are in the range of (1.01-11.9) x 10^{-6}A/sq.cm and (1.05-11.6) 10^{-6}A/sq.cm at temperatures 30 and 65°C respectively.

2. The value of the exchange current density is found to be a little higher than that reported in the literature. The situation suggests that the electrodes used for this investigation have higher performances.

3. An increase in temperature leads to an increase of the exchange current density and hence an increase of the performance of the electrodes.

4. The range of the values of the double layer capacitance was found to be (91 – 104)μf. for the exponential current decay method. The values obtained by using the triangular wave of current are also in the range of (167 – 294)μf. This confirms the earlier conclusion that an increase in temperature leads to an increase in the electrode performance.

5. The Surface Roughness Factor determined at 65°C is $34 \times 10^{-3} cm^2/cm^2$. The value obtained by Rangarajan at 80°C is $25 \times 10^{-3} cm^2/cm^2$. Again the improved electrode structure gave better surface utilization.

6. The value of the activation energy was found to be 4.15 kcal/gmol. The range of values in the literature is (5.23 - 10) kcal/gmol. The low activation energy obtained is due to the new preparation technique.

7. The exponential decay current technique is a more suitable method for determining the electrodes parameters. The method gives the physical explanation for some of the observed features.

6.2 Recommendations for Further Work

The specific objectives of this thesis work were to determine the exchange current density, the double layer capacity and the specific surface area of the electrodes used in the alkaline fuel cell. These were achieved. However, there is much work to be accomplished in order to bring the whole concept of fuel cell to a practical realisaton.

It is therefore recommended that the following be persued:

1. The electrodes should be fabricated at KFUPM

2. Incorporate the role of mass transport in further studies.

3. Finally, the effects of the electrolyte concentration on the exchange current density be investigated.

REFERENCES

1. Young C.J.,"Fuel Cells,"Reinhold Publishing Co., NewYork, 1960.

2. Organising Committee," A Three Day Simposium-Energy Production Processes. The Institute of Chemical Engineers:Warwickshire. April 12-14 1988.

3. Benjamin,T.G..Camara,E.H.,Marianowski,L.G.,"Handbook of Fuel Cell Performance"USDOE, contract No.EC-77-C-03-1545, 1980.

4. Geoffrey,Prentice, A., "Fuel Cells: Principles and Prospects" Chemtech, Nov.1984.

5. Liebhafsky,H.A. and Carins, E.J. Fuel Cells and Fuel Batteries John Wiley:Newyork,1986.

6. Thallar, L.H., Martin, R.E. and Stadman J. K., "Stress-Life Interrelationships Associated with Alkaline Fuel Cells" 22nd Annual IECEC Conference,Philadelphia,1987.

7. "The Gas Powercel National Market Report: Characterization of the on-site Fuel Cell Market."Onsite Fuel cell Users Group,Market Business Asessment Task Force,Dec. 1985.

8. Energy and Environmental Analysis Inc."Distribution of Methanol for Motor Vehicle Use in the California South Coast Air Basin."September,1986.

9. Gallagher-Daggitt,G. "The Status of Research and Application of Fuel Cells in the U.K. Fuel Cells:Trends in Research and Applications. Hemisphere Publishing Corp.1987.

10. Cowley,S.W.and Gebhard,S.C."The Catalytic Decomposition of Methanol into Synthetic Gas for Use as an Automative Fuel."Solar Energy Research Instsitute, ColoradoSchool of Mines, Report No.0163-9153/83/ 7803-0041.

11. Grant, T. J. and Estereich,P.J. "Site Specific Fuel Cell/ Coal Gasification Plant Designs."Fuel Cell Seminar, TUCSON Az, 1986.

12. Penner,S.S.,"Assesment of Reasearch Needs for Advanced Fuel Cells by the DOE Advanced Fuel Cell Working Group(AFCWG)." USDOE contact No. DE-AC01-84ER300[illegible],Nov.1985

13. Russel,J.H.,Proceedings of the 19th Power Sources Conference PSC Publications,vol. 35,1965.

14. Morril, C.C.,Proceedings of the 19th Power Sources Conference PSC Publications , Vol.35,1965

15. Sandatede,G. Form Electrocatalysis to Fuel Cells,Bettelte Seatle Reseach Center and the Univ. of Washington Press:USA 1972.

16. Nuttal,L.J. Titterngton,W.A.,"Conference on the Electrolytic Production of Hydrogen." City Univ. London,1975.

17. Boretz,John,E."Space Power Alternatives for Laser Radar Sensor

System."Electrochemical Storage and Conversion,24th IECEC, vol.3 Washington D.C.August6-11,1989.

18. Warshang,M."Status of Commercial Fuel Cell Power Plants System Development" 22nd Annual IECEC Conference,Philadelphia,1987.

19. Rastler,D."Phosphoric Acid Fuel cell Commercialization Activities in the United States"Fuel Cell Technology and Aplications International Seminar,The Netherlands,1987.

20. Ching A.C.,Gillis,A.P., Plauche,F.M.,Proceedings of 7th Intersoc.Energ. Conv. Eng. Conf. Vol.368,(1972).

21. Handley,L.M.,Mary G.W.,"The PC 23 Fuel Cell-A Strategic Alternative, Fuel Cell Seminar, TUCSON AZ,1986.

22. Newby,D.,"The Westinghouse 1.5MW Fuel Cell Pilot Plant-The Next Step to Commercialiazation ."Fuel Cell Seminar ,TUCSON AZ, 1986.

23. Sabbioni,F. Imbimbo,E.DIgnazio P.D. etal "Phosphoric acid Fuel Cell for Electrical Power Generation: Development and Penetration in the EEC Countries".Commission of the European Communities,Energy Final Report,1986.

24. Ove Arup and Partners,"Potential Market for Fuel Cell CHP"Johnson Matthey PLC internal Report,January 1987.

25. Linden,D.,Handbook of Batteries and Fuel Cells,McGraw Hill New York,1983.

26. Gileady, E. et al Interfacial Electrochemistry: An Experimental Approach. Addison-Wesley Publishing Company,Inc. Massachusetts,1975.

27. Gouy, A., J. Phys. 4,9,457(1910)

28. Rangarajan, S.K.,J.Electrochem.Soc.111,799(1964)

29. Bockris, J.M. and Conway B.E.,"Modern Aspects of ElectroChemistry." No.5,Premium Press NewYork,1969.

30. Allen, Bard J. and Faulkner, Electrochemical Methods: Fundamentals & Applications. John Wiley & sons, Inc. New York,1980.

31. Tilak, B.V.,Yeo, R.S. and Srinivascan,S., Comprehensive Treatise of Electrochemistry, Olenum Press, Vol.39, No. 3, 1981.

32. Crow, D.R."Principles and Applications of Electrochemistry" Chapman and Hall ltd, 11New Fetterlane, London 1974.

33. Bokris,J.O'M. and Srinivascan,S., Fuel Cells:Their ElectroChemistry: McGraw Hill. New York, 1969.

34. Tilak, B. V., Radar C.G. and Rangarajan, S.K., "Techniques for Characterizing Porous Electrodes " J. Electrochem.Soc., 124, 1879 (1977).

35. Tilak, B. V.,and Rangarajan,S.,K.,"On Determining the Double Layer Capacity of Porous Electrodes"Transactions of SAEST, vol.13, no.4, 1978.

36. Vetter, K.G., Electrochemiche Kinetik, Springer Verlag, Berlin (1961).

37. Daniel'-Bek, V.S., Zhur Fiz. Khim 20, 567 (1964).

38. Weisselberg et al,Trans. Electrochem. Soc.,90, 235 (1946).

39. Waber, J.T., and Rosenbluth, M., J.Electrochem.Soc.102, 344, (1955).

40. Frumklim, A.N.; Zhur,Physik Chem. 164,121(1933).

41. Ksenzhek, O.S., Russ. J. Phys. Chem.37, 2007 (1963)

42. Winsel,A., Zh. Eletrktrochem. 66, 287 (1964).

43. Posey,F.A., "Methods for the Calculation of Polarization in Porous Electrodes"J.Electrochem.Soc.,111,1173,(1964).

44. Macdonald, Digby D., Transient Techniques in Electrochemistry. Newyork: Plenum Press, 1977.

45. Erdey-Gruz, Tibor, Kinetics of Electrode Processes. London:

46. Gerischer, H. , Anal. Chem. 31,33 (1959).

47. Gerischer, H. and Vielstich W.:, Anal. Chem. 3,16(1955).

48. Randles, J.E.B., Trans. Faraday Soc. 44,327,(1948).

49. Cottrell,F.G.,Zhu.,Phys. Chem. 42,385(1903).

50. Delahay, P.,J.Amer. Chem. Soc. 75,1190(1953).

51. Nicholson, R.S. and Shain, Anal. Chem.36,706,(1964)

52. Gokhshtein,A.Y., Doklady Akad. Nauk SSSR 131,601(1960)

53. Saveant,J.M. and Vianello, E., Electrchem. Acta, 8 905 (1963)

54. Will,F.G. and Knorr, C.K.,Zh. Elektrochem. 64,258(1960).

55. Conway, B.E.and Gileadi E. Trans Faraday Soc.58,2493,(1962).

56. Hale,J.M. and Greef, R., Electrochem. Acta ,12 1409 (1967).

57. Ksenzhek, O.S.,and Stender,Russ. J. Phys. Chem. 31,117 (1957)

58. Ksenzhek. O.S.,and Stender,V.V.,Dokl. Arad Nark S.S.S.R, 106,481(1956).

59. Ksenzhek, O.S.,Russ. J. Phys.Chem. 38,1846(1964)

60. Posey,F.A. and Morozumi,T."Theory of the Potentiostatic and Galvanostatic Charging of the Double Layer in Porous Electrodes"J.Electrochem.Soc.,113,176,(1966).

61. Tiedmann, W.,and Newmann,J.,J.Electrochem.Soc.,122,70, (1975).

62. Rangarajan,S.K.,"Theory of Flooded Porous Electrodes." Electroanalytical Chem. and Interfacial Electrochem.,22, 89-104,(1973).

63. Guruvich, I.G. and Bagotski, V.S.,Elektrokhimiya,1,1102 (1965).

64. Rangarajan,S.K.,"On Linear Relaxation Methods." Electroanalytical Chem. and Interfacial Electrochem.,41, 459-471,(1973).

65. De Levie, R.,"Electrochemical Response of Porous and Rough

Electrodes." Adv. Electrochem. Eng. Vol.6 329,(1967).

66 Austin, L.G.and Gagnon E.G.,"The Triangular Voltage Sweep Method for Determinig Double Layer Capacity of Porous Electrodes."J. Electrochem.Soc.121,251(1973).

67. Muud,Konrad,Edling Martin and Ritcher Gerhard, 'Impedence Measurements with Porous Electrodes for Electrochemical Energy Conversion and and Storage."Siemens Research and Developments Reports.1982.

68. Lu,P.W.T., and France, L.L.,' Effects of Gas-phase Transport on the Performance of Laminated Fuel Cell Cathodes.'NASA-Lewis Research Center Contract No. DEN 3-161.

69. Hobbs D.S., Vassie P.R. and Tseng A.C.C."The Application of Pulse Technique to the Study os Porous Electrodes"

70. Kantan,T.,and Carlen,P.J.,' Pertubations and Relaxation of Concentration Gradients in Porous Zinc Electrodes Department of Contract No.S/C 4563610.

71. Rangarajan,S.K.,"An Exponential Relaxation Technique." Electroanalytical Chem. and Interfacial Electrochem.,41, 491-502,(1973).

72. Rangarajan,S.K. et al, "Techniques for Characterizing Porous Electrodes"J.Electrochem.Soc.,124,1879 (1977).

73. Celiker. H., Ph. D Thesis, King Fahd University of Petroleum and

Minerals. Dhahran 1990.

74. De Levie, R.,"On Porous Electrodes in Electrolyte Solutions-IV."Electrochim. Acta,9,1231(1964).

APPENDIX A

TABLE A.1: Results of Overpotential andCurrent Density during Activation.

Open Cell Voltage (OCV) : -928.9mV

Area of Electrode : 6sq.cm

Temperature : 24 Deg. C

Current Density	Electrode potential (With IR Drop)mV		IR Drop	Overpotential (IR Drop Free)mV	
(mA/sq.cm)	Forward	Backward	(mV)	Forward	Backward
2	-922.3	-922.0	3	3.6	3.9
4	-913.9	-912.5	11	3.9	4.0
6	-906.2	-906.4	15	7.7	7.5
8	-898.1	-898.5	20	10.8	10.4
10	-890.2	-890.9	27	11.7	11.0
12	-881.8	-881.1	34	13.1	13.8
14	-873.4	-873.5	38	17.5	17.4
16.7	-862.6	-862.3	46	20.3	20.6
21.7	-842.6	-842.2	60	26.3	26.7
26.3	-821.7	-821.4	70	37.2	37.5
33.3	-794.6	-794.1	92	42.3	42.8
38.3	-774.7	-774.2	100	54.2	54.7
41.7	-760.9	-760.8	110	58.0	58.1
46.7	-739.8	-739.6	126	63.1	63.3
50.0	-725.5	-725.4	134	69.4	69.5
56.7	-697.7	-697.4	148	83.2	83.5
63.3	-670.2	-670.3	166	92.7	92.6

TABLE A.2: Results of the Input Pulse for the Exponential Decay Current

Temperature : 30 Deg. C

Capacitance (uf)	Reading from oscillioscope		
	Ampl./Div.(mV)	Time/Div.(us)	No. of divisions (Δi)
0.01	20	50	1.8
0.047	20	50	3.4
0.22	20	50	4.3
0.47	20	50	4.5
1.00	20	50	4.6
2.2	20	0.1	1.9

TABLE A.3: Results of the Input Pulse for the Exponential Decay Current

Temperature : 42 Deg. C

Capacitance (uf)	Reading from oscillioscope		
	Time/Div.(us)	Ampl/Div.(mV)	No. of Div. (Δi)
0.01	20	50	1.8
0.047	50	50	1.4
0.22	50	50	1.8
0.47	50	50	1.9
1.00	50	50	1.9
2.2	20	50	2.0

TABLE A.4: Results of the Input Pulse for the Exponential Decay Current

Temperature : 48 Deg. C

Capacitance (uf)	Reading from oscillioscope		
	Time/Div.(us)	Ampl/Div.(mV)	No. of Div. (Δi)
0.01	20	20	1.9
0.047	50	50	1.4
0.22	50	50	1.7
0.47	50	50	1.9
1.00	50	50	1.9
2.2	50	50	2.0

TABLE A.5: Results of the Input Pulse for the Exponential Decay Current

Temperature : 65 Deg. C

Capacitance (uf)	Reading from oscillioscope		
	Time/Div.(us)	Ampl./Div.	No. of divisions (Δi)
0.01	50	50	0.8
0.047	50	50	1.4
0.22	50	50	1.8
0.47	50	50	2.0
1.00	50	50	2.2
2.2	50	50	2.3

TABLE A.6: Results of the Response to the Exponential Decay Current

Temperature : 30 Deg. C

T/D:Time per division

Ampl: Amplitude

Capacitance (uf)	Reading from oscillioscope			
	T/D(ms)	Ampl(mV)	Height	Length
0.01	0.5	10	0.2	3.0
0.047	0.5	50	0.4	4.0
0.22	0.5	50	2.0	4.8
0.47	0.5	50	4.1	5.7
1.00	0.5	50	5.7	6.0
2.2	0.5	50	6.0	6.7

TABLE A.7: Results of the Response to the Exponential Decay Current

Temperature : 42 Deg. C

T/D:Time per division

Ampl: Amplitude

Capacitance (uf)	Reading from oscillioscope			
	T/D(ms)	Ampl(mV)	Height	Length
0.01	0.5	0.2	2.0	
0.047	0.5	50	0.3	4.2
0.22	0.5	50	2.0	6.4
0.47	0.5	50	4.3	7.6
1.00	0.5	50	8.8	9.4
2.2	0.5	50	11.2	10.2

TABLE A.8: Results of the Response to the Exponential Decay Current

Temperature : 48 Deg. C

T/D:Time per division

Ampl: Amplitude

Capacitance (uf)	Reading from oscillioscope			
	T/D(ms)	Ampl(mV)	Height	Length
0.01	0.5	10	0.2	2.6
0.047	0.5	50	0.3	5.0
0.22	0.5	50	1.7	6.8
0.47	0.5	50	3.9	7.0
1.00	0.5	50	7.6	9.9
2.2	0.5	50	13.3	11.9

TABLE A.9: Results of the Response to the Exponential Decay Current

Temperature : 65 Deg. C

T/D:Time per division, Ampl: Amplitude

Capacitance (uf)	Reading from oscillioscope			
	T/D(ms)	Ampl(mV)	Height	Length
0.01	0.5	20	0.1	2.6
0.047	0.5	20	0.8	4.4
0.22	0.5	20	4.3	6.6
0.47	0.5	20	9.5	6.0
1.00	0.5	50	4.5	10.6
2.2	0.5	50	5.1	12.1

TABLE A.10: Values of $\ln\frac{\eta_{max}}{\Delta i\ \tau}$ (LNDIMAX) and t_{max} (TMAX)

Temperature : 30 Deg. C

LNDIMAX (ω/S)	TMAX 10^4
9.90	15.0
9.60	20.0
8.85	24.1
8.30	28.5
7.95	30.0
7.20	35.5

TABLE A.11: Values of $\ln\frac{\eta_{max}}{\Delta i\ \tau}$ (LNDIMAX) and t_{max} (TMAX)

Temperature : 42 Deg. C

LNDIMAX (ω/S)	TMAX 10^4
9.60	10.0
8.70	21.0
8.15	32.4
7.65	38.1
6.60	47.0
5.40	59.0

TABLE A.12: Values of $\ln\frac{\eta_{max}}{\dot{\Delta i}\,\tau}$ (LNDIMAX) and t_{max} (TMAX)

Temperature : 48 Deg. C

LNDIMAX (ω/s)	TMAX 10^4
8.60	13.0
7.00	25.0
6.40	34.0
6.00	35.1
5.00	49.5
3.40	59.3

TABLE A.13: Values of $\ln\frac{\eta_{max}}{\Delta i\ \tau}$ (LNDIMAX) and t_{max} (TMAX) Temperature : 65 Deg. C

(LNDIMAX) (ω/S)	TMAX 10^4
7.85	13.0
7.15	22.0
6.00	33.2
5.15	30.4
1.60	53.0
1.05	60.6

TABLE A.14: Results for the Exponential Decay Current Technique

EXCDENSITY :Exchange Current Density

DOBLACAPACITY:Double Layer Capacity

Temperature (°C)	EXCDENSITY $(Amps/cm^2)*10^6$	DOBLACAPACITY (μF)
30	4.00	91
42	6.42	93
48	9.28	98
65	11.90	104

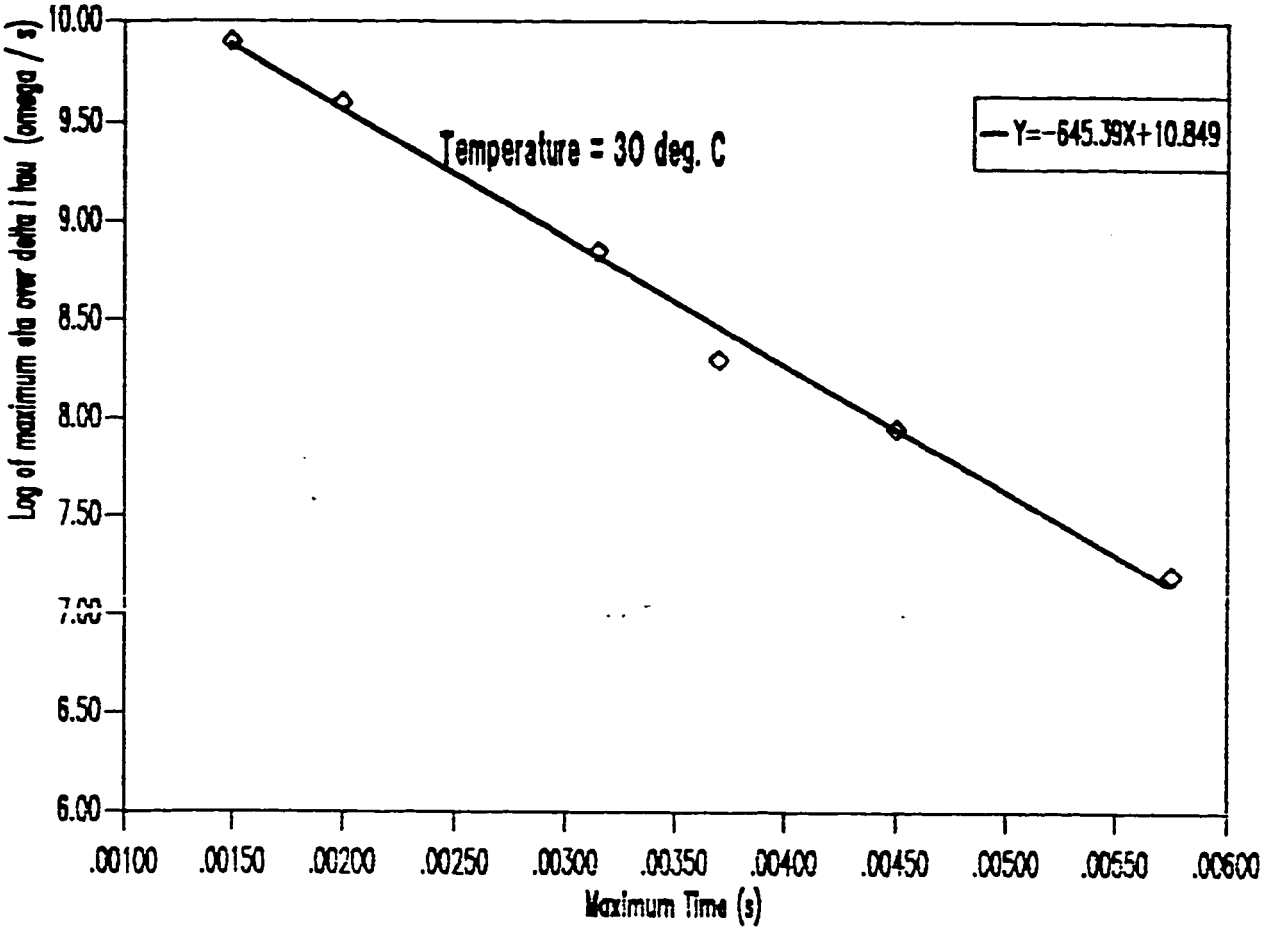

Figure A.1: Plot for the exponential decay current at 30 deg. C

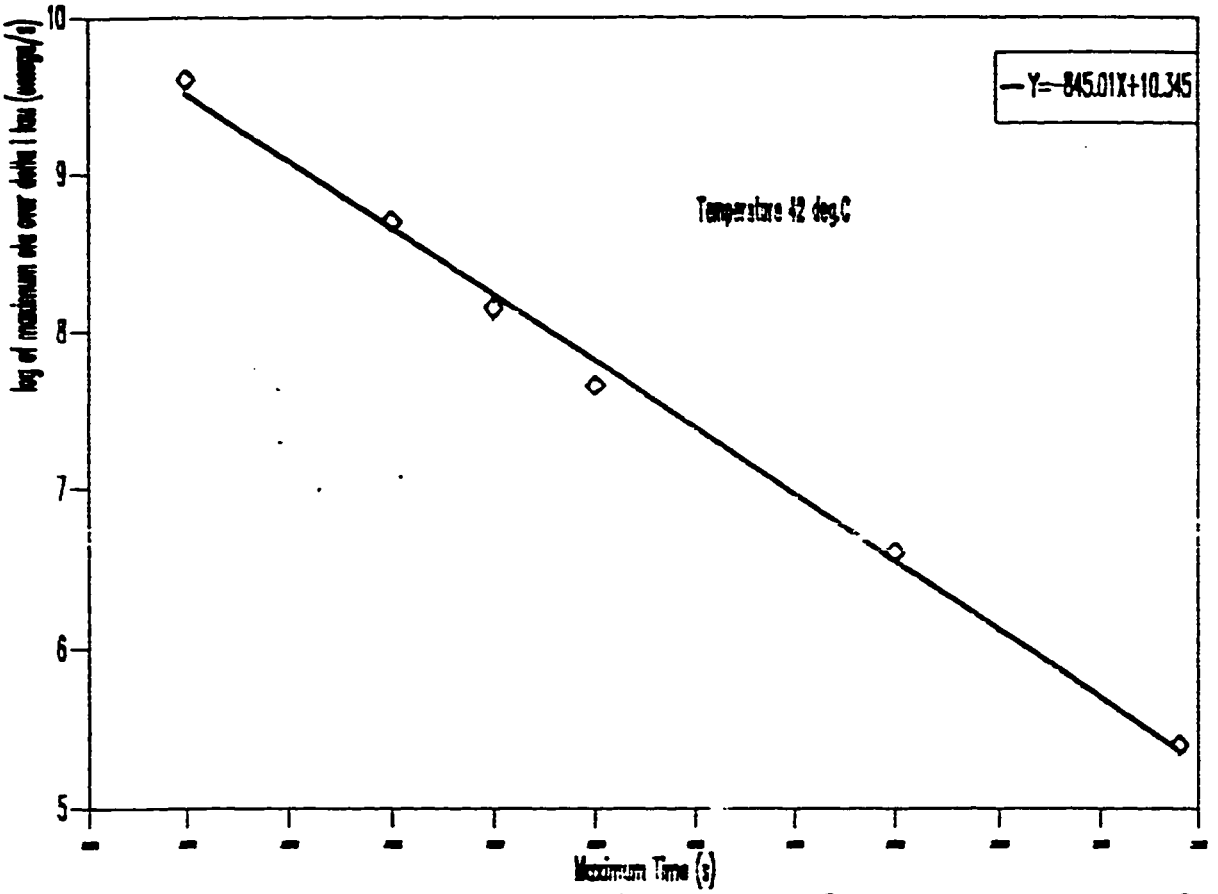

Figure A.2: Plot of Exponential Decay Current at 42 deg.C

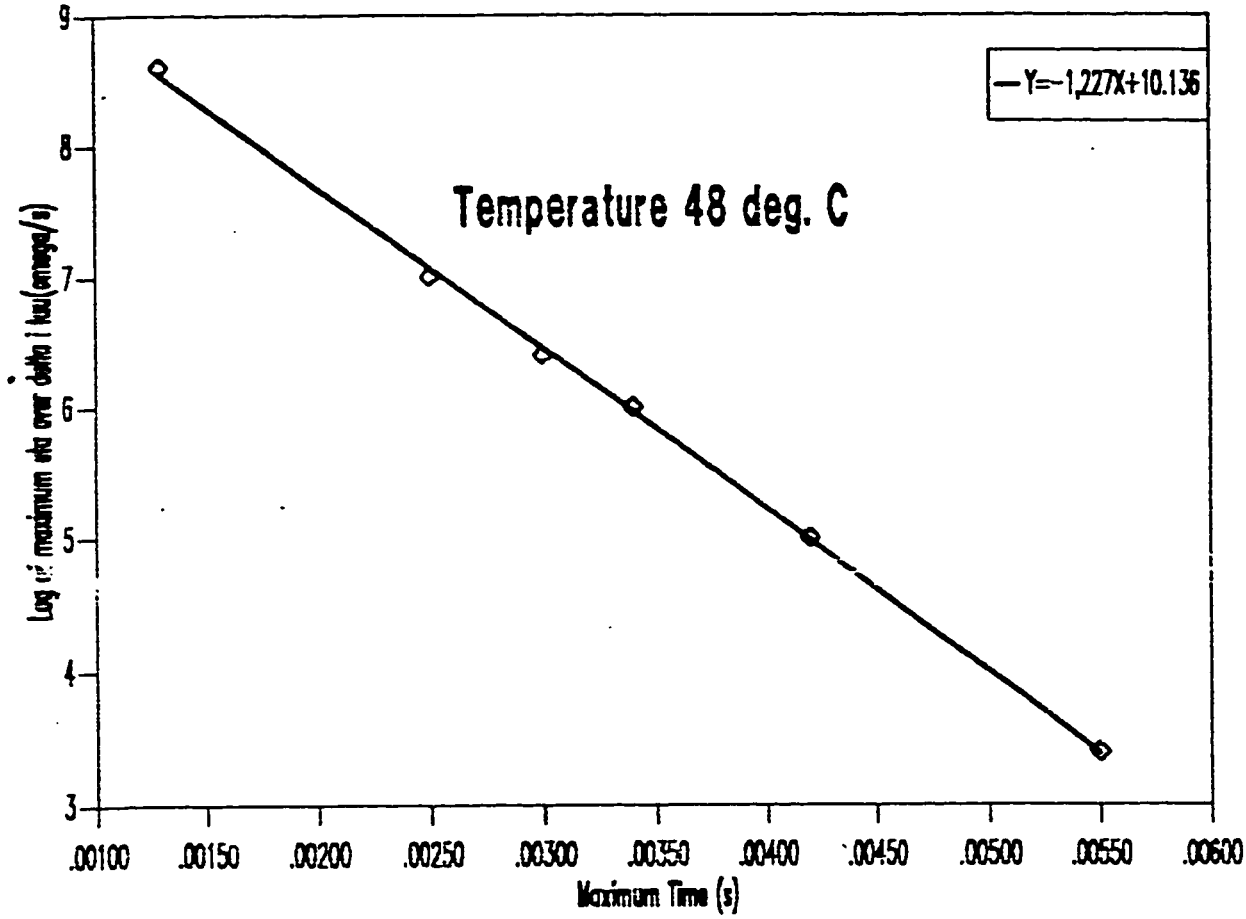

Figure A3: Plot of the Exponential Decay currentat 48 deg. C

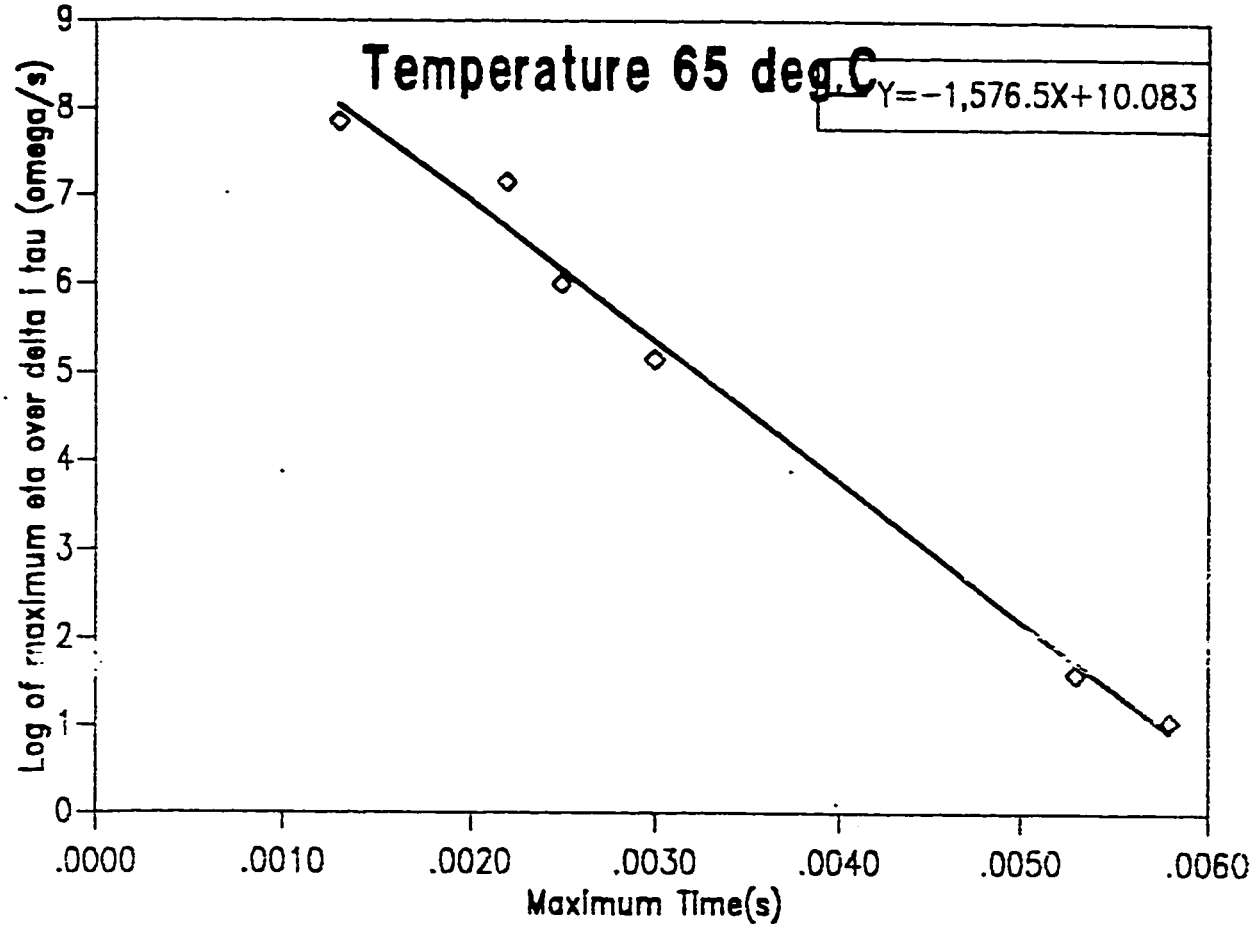

Figure A.4 Plot of the Exponential Decay Current at65 deg. C

APPENDIX B

SAMPLE CALCULATION

DATA :

Specific surface area = 3.6 sq.m/g

Thickness of electrode = 2.70×10^{-4}m

Mesh weight = 0.1903g

Active electrode = 0.3787g

Conductance of KOH solution:

$$\sigma = 0.0262W + 0.00067W\,t - .00048W^2 - 0.0000088W^2t$$

Temperature for the sample calculation = 30°C

1. Exponentiai Decay Current Method

A. The gradient from the plot (computer fit) $\ln \frac{\eta_m}{\Delta i\,\tau}$ versus t_{max}

$$= -645.39 \frac{\Omega}{s^{-2}}$$

B. The intercept $= \frac{1}{C_T}$

$= 10.9\Omega ms^{-1}$ and

$C_T = 91mF$

C. Exchange Current Density

From the relationship

$$\text{Gradient (slope)} = \frac{\alpha}{\beta} = m$$

$$= \frac{R_o L n S F i_o}{R T^* R_o C_T}$$

Hence,

$$i_o = \frac{m R T C_T}{L Sn F}$$

$$= \frac{645.4x8.314^*303^*91x10^{-3}}{(\frac{3.6}{0.3787})^*4^*96500} A/m^2$$

$$= 4.01X10\text{-}6A/cm^2$$

2. Triangular Wave Current Method.

A triangular wave galvanostatic transient at low frequencies i.e. $t > t_o$.

will give the current wave as

$$i(t) = \mu t \ (0 <= t < \frac{T}{2})$$

$$i(t) = \mu(T-t) \ (\frac{T}{2} <= t < T)$$

For $T >> t$ equation (12) gives the maximum potential excursion and then,

$$\frac{\eta(0,\frac{T}{2})}{i(\frac{T}{2}) R_o} = \frac{T}{4\tau}$$

Temperature = 30 deg. C

$$i(\frac{T}{2}) = 54mA$$

Period(T) = 180s

$\eta(0,T_2)$ = 1.347V

Conductance of the KOH solution at 30°C = $7.48 \times 10^{-5} \Omega^{-1} cm^{-1}$

Hence, $R_o = \frac{l}{\sigma A}$

$$= 2.7x\frac{10^{-6}}{6.0x7.48x10^{-5}}$$

$$= 6.014x10^{-3}\ \Omega$$

Now, from the potential equation $\tau = T * i\frac{R_o}{4*\eta}$

$$= \frac{0.0054*180*6.014x10^{-3}}{1.347*4}$$

$$= 1.085*10^{-3}s$$

But $\tau = R_o*C_T$

$$C_T = \frac{\tau}{R_o}$$

$$= 1.08\ 5x\frac{10^{-3}}{6.498x10^{-3}}$$

$$= 167mF$$

A. Calculation of the exchange current density

A charge transfer controlled reaction is given by

$$i(t) = C_T\frac{d\eta}{dt} + i_o\, n\, F\, \frac{\eta}{RT}.$$

The exchange current density is then given by

$$i_o = \frac{\{C_r \frac{d\eta}{dt} - i\}RT}{n F \eta}$$

$$= \frac{0.167 * \frac{0.42}{6x180} * \{ - \frac{0.0054}{6}\} * 8.314 * 303}{4 * 96500 * (-1.347)}$$

$$= 4.05x10^{-6} A/cm^2$$

3. Determination of Activation Energy

The equation for the activation energy relationship is given as :

$$\ln i_o = K - \frac{U_e}{RT}$$

A slope from the plot of $\ln i_o$ versus $\frac{1}{T}$ is :

$$= 3.5x10^3 K$$

$$= \frac{U_e}{R}$$

Therefore,

$$U_e = 3.5X10^3 * 1.187 calg\text{-}mol^{-1}K = 4.15Kcal/gmol$$

Determination of surface roughness factor

The capacitance per unit area is related to the total capacitance by the relationship

$C_T = SCl$

and

$$C = \frac{C_T}{Sl}$$

$$RF = \frac{C}{C_{ideal}}$$

Temperature : 30°C

$C_{ideal} = 1.7 \times 10^{-5} \mu/cm^2$

Therefore,

$$RF = \frac{167 \times 10^{-3}}{270 \times 10^{-4} * 1 \times 10^{-6}} \frac{cm^2}{cm^2}$$

$$= 36 \times 10^4 \frac{cm^2}{cm^2}$$

APPENDIX C

Derivations of Equations for the Model of Exponential Decay Current.

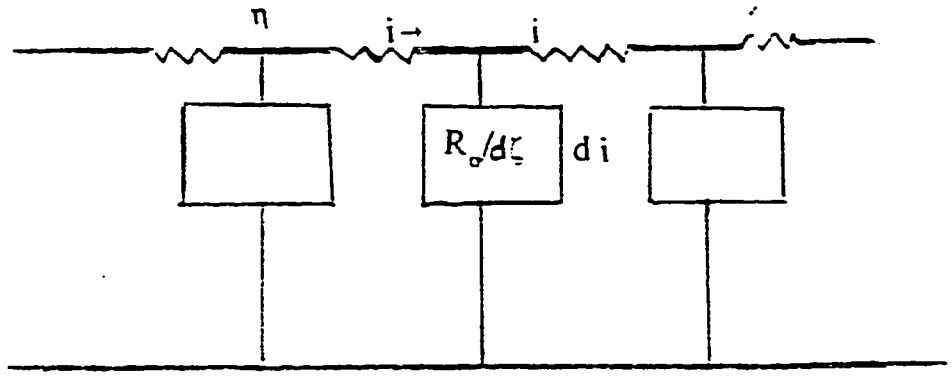

Figure (C1): Single Pore Equivalent Circuit Representation

where

$d\zeta$:Small section of equivalent pore

η:Overpotential

ζ:Distance

i : Current

R_o:Electrode impedence

PART A

The approach that will be discussed here has been extensively treated by De levie{74}. The model for the exponential decay current can be closely viewed as in figure C.1. In this figure, the electrode system is represented like a series of resistances in the form of a transmission line. We start by giving the elementary current relationship. For sufficiently small changes of potential (so that the double layer capacitance C is constant), the local current density is given by:

$$di = \partial i/\partial \zeta \; d\zeta$$

$$= C \, \partial \eta/\partial t \, d\zeta \qquad (C1)$$

Alternatively we write equation C1 as,

$$\frac{\partial i}{\partial \zeta} = C \frac{\partial \eta}{\partial t} \qquad (C2)$$

Similarly, the potential is given by

$$d\eta = -i R_o \, d\zeta \qquad (C3)$$

This can also be re-written as

$$\frac{d\eta}{d\zeta} + i R_c = 0 \qquad (C4)$$

Denoting the instantaneous and equilibrium concentrations of the reactants(R) and products(P) as $C_i(x,t)$ and $C_i^v (i = R,P)$ respectively, a Volmer type expression is used to describe the local faradaic current density as

$$\frac{ij}{i_o} = [(C_r/C_r^v)\exp(\alpha_c F\eta/RT) - (C_p/C_p^v)\exp(\alpha_c - n)F\eta/RT)] \qquad (C5)$$

In equation C5 a linearization is achieved by substituting

$$n = \alpha_c + \alpha_a$$

and then considering the fact that there is near equilibrium conditions so that we have constant concentration. Equation C6 is then obtained as the linearised form of the Volmer eqation.

$$i = \frac{i_o n F \eta}{RT}. \qquad (C6)$$

Combining equations C2 and C4 gives

$$\frac{\partial^2 \eta}{\partial \zeta^2} - R_o C \frac{\partial \eta}{\partial t} = 0 \qquad (C7)$$

Equation C7 is the equation governing the distribution of potential in the electrode pore. Now, the potential due to the faradaic currents (i) along the entire length (l) of the pore is

$$\eta_r = i R_o S l \qquad (C8)$$

Substituting for j from equation C6 in equation C7 and incorporating the result in the potential distribution equation leads to

$$\frac{\partial^2 \eta}{\partial \zeta^2} - \frac{i_o n F R_o S l \eta}{RT} - R_o C \frac{\partial \eta}{\partial \zeta} = 0 \qquad (C9)$$

Combining all constants lead to equation

$$\frac{\partial^2 \eta}{\partial \zeta^2} - \alpha \eta - \beta \frac{d\eta}{dt} = 0 \qquad (C10)$$

where $\alpha = R_o \frac{slnFi_o}{RT}$

and $\beta = R_o C_T$

Equation C10 is equation 38 given earlier without derivation.

PART B

Referring to figure 3.1 the following system of differential equations can be formulated.

I. C.

$$\eta(\zeta=0) = 0 \qquad \text{(C11)}$$

Boundary conditions:

B.C.1

$$\frac{\partial\eta}{\partial\zeta}(1,t)=0 \qquad \text{(C12)}$$

B.C.2

$$\frac{\partial\eta}{\partial\zeta}(0,t)= -R_o i(t) \qquad \text{(C13)}$$

where i(t) is given by equation 34 as $i(t) = \Delta i \exp(-\frac{t}{\tau})$

Substituting the expression of i(t) in equation C13 gives

$$\frac{\partial\eta}{\partial\zeta}(0,t)= -\Delta i R_o \exp(-t/\tau) \qquad \text{(C14)}$$

The solution to the differential equations is obtained by using Laplace transformations. Therefore defining the Laplace transform as $\bar{f}(x,s) = \int_0^\infty e^{st} f(x,t)dt$, we take the Laplace transforms of all of the system of differential equations. Equations C12 to C13 are therefore

transformed as follows.

The transform of equation C11 is given as

$$\frac{d\bar{\eta}}{d\zeta}(1,s)=0 \qquad (C16)$$

and from equation C14 we have

$$\frac{d\bar{\eta}}{d\zeta}(0,s) = = -R_o\bar{\sigma i}\left(\frac{1}{s+1/\tau}\right) \qquad (C17)$$

Finally, the Laplace transform of the overpotential equation C15 gives

$$\frac{d^2\bar{\eta}}{d\zeta^2} - \alpha\bar{\eta} - \beta\{s\bar{\eta} - \eta(\zeta,0)\} \qquad (C18)$$

Substituting the initial condition and simplifying gives

$$\frac{d^2\bar{\eta}}{d\zeta^2} - (\alpha + \beta s)\bar{\eta} = 0. \qquad (C19)$$

Applying the Laplace transformation technique,we have converted the partial differential equations to ordinary differential equations. Equation C19 is a linear differential equation with roots $- + 1/2(\alpha + \beta s)^{1/2}$. The general solution of the equation is given by

$$\bar{\eta} = A_1 \cosh 1/2(\alpha+\beta s)^{1/2}\zeta + B_1 \sinh 1/2(\alpha+\beta s)^{1/2}\zeta \qquad (C20)$$

Where A_1 and B_1 are constants. We now determine the the constants by substituting the boundary conditions. First of all, differentiate

eqution C20 with respect to ζ to get

$$\frac{d\eta^-}{d\zeta} = A_1 1/2(\alpha+\beta s)^{-1/2}\sinh 1/2(\alpha+\beta s)^{1/2}\zeta + B_1(\alpha+\beta s)^{1/2}\cosh 1/2(\alpha+\beta s)^{1/2}\zeta \quad \text{(C21)}$$

Now substitute boundary condition 2 and for $\zeta=0$ we obtain B1 as

$$B_1 = \frac{-2R_e\Delta i}{(s+1/\tau)(\alpha+\beta s)^{1/2}} \quad \text{(C22)}$$

Next, substituting boundary condition 1 into the solution of the general equation and making use of B_1 while noting the fact that $\zeta=1$, the constant A_1 is given as

$$A_1 = 2R_e\Delta i\cosh 1/2(\alpha+\beta s)^{1/2} - (s+1/\tau)(\alpha+\beta s)^{1/2}\sinh 1/2(\alpha+\beta s)^{1/2} \quad \text{(C23)}$$

Now substituting the values for the constants A_1 and B_1 into the general equation, we obtain the Laplacian form of for the over potential given by

$$\eta^- = \frac{R_o\Delta i\cosh\frac{1}{2}(\alpha+\beta s)}{(s+1/\tau)\sinh\frac{1}{2}(\alpha+\beta s)}\left[\frac{2\cosh 1/2(\alpha+\beta s)^{1/2}\zeta}{(\alpha+\beta s)^{1/2}1/2(\alpha+\beta s)^{1/2}} - \frac{\sinh 1/2(\alpha+\beta s)^{1/2}\zeta}{(\alpha+\beta s)^{1/2}\cosh 1/2(\alpha+\beta s)^{1/2}}\right] \quad \text{(C24)}$$

Finally, we look up tables (60) for the inverse Laplacian transform and rearrange to get equation 39 as shown earlier without detailed solution.

$$\eta = -R_o i(t)\left\{\left[\exp\frac{(-t(B-\frac{1}{\tau}))-1}{\beta(B-\frac{1}{\tau})}\right] + \left[\frac{2}{\beta}\sum_{n=1}^{\infty}\frac{(-1)^n\cos n\pi(1-\varepsilon)\,(\exp(t(A-\frac{1}{\tau}))-1)}{(A-\frac{1}{\tau})}\right]\right\} \quad \text{(C25)}$$